
This is an electronic reprint of the original article.
This reprint may differ from the original in pagination and typographic detail.

Tekgül, Bulut; Kahila, Heikki; Kaario, Ossi; Vuorinen, Ville
Large-eddy simulation of dual-fuel spray ignition at different ambient temperatures

Published in:
Combustion and Flame

DOI:
[10.1016/j.combustflame.2020.01.017](https://doi.org/10.1016/j.combustflame.2020.01.017)

Published: 01/05/2020

Document Version
Publisher's PDF, also known as Version of record

Published under the following license:
CC BY-NC-ND

Please cite the original version:
Tekgül, B., Kahila, H., Kaario, O., & Vuorinen, V. (2020). Large-eddy simulation of dual-fuel spray ignition at different ambient temperatures. *Combustion and Flame*, 215, 51-65.
<https://doi.org/10.1016/j.combustflame.2020.01.017>

This material is protected by copyright and other intellectual property rights, and duplication or sale of all or part of any of the repository collections is not permitted, except that material may be duplicated by you for your research use or educational purposes in electronic or print form. You must obtain permission for any other use. Electronic or print copies may not be offered, whether for sale or otherwise to anyone who is not an authorised user.



Large-eddy simulation of dual-fuel spray ignition at different ambient temperatures



Bulut Tekgül*, Heikki Kahila, Ossi Kaario, Ville Vuorinen

Department of Mechanical Engineering, Aalto University School of Engineering, Otakaari 4, Espoo 02150, Finland

ARTICLE INFO

Article history:

Received 20 December 2018

Revised 22 July 2019

Accepted 18 January 2020

Keywords:

Large-eddy simulation

Dual-fuel

Ignition

IDT

Ambient temperature

ECN Spray A

ABSTRACT

Here, a finite-rate chemistry large-eddy simulation (LES) solver is utilized to investigate dual-fuel (DF) ignition process of *n*-dodecane spray injection into a methane–air mixture at engine-relevant ambient temperatures. The investigated configurations correspond to single-fuel (SF) $\phi_{\text{CH}_4} = 0$ and DF $\phi_{\text{CH}_4} = 0.5$ conditions for a range of temperatures. The simulation setup is a continuation of the work by Kahila et al. (2019, *Combustion and Flame*) with the baseline SF spray setup corresponding to the Engine Combustion Network (ECN) Spray A configuration. First, ignition is investigated at different ambient temperatures in 0D and 1D studies in order to isolate the effect of chemistry and chemical mechanism selection to ignition delay time (IDT). Second, 3D LES of SF and DF sprays at three different ambient temperatures is carried out. Third, a reaction sensitivity analysis is performed to investigate the effect of ambient temperature on the most sensitive reactions. The main findings of the paper are as follows: (1) DF ignition characteristics depend on the choice of chemical mechanism, particularly at lower temperatures. (2) Addition of methane to the ambient mixture delays ignition, and this effect is the strongest at lower temperatures. (3) While the inhibiting effect of methane on low- and high-temperature IDT's is evident, the time difference between these two stages is shown to be only slightly dependent on temperature. (4) Reaction sensitivity analysis indicates that reactions related to methane oxidation are more pronounced at lower temperatures. The provided quantitative results indicate the strong ambient temperature sensitivity of the DF ignition process.

© 2020 The Author(s). Published by Elsevier Inc. on behalf of The Combustion Institute.

This is an open access article under the CC BY-NC-ND license.

(<http://creativecommons.org/licenses/by-nc-nd/4.0/>)

1. Introduction

Engine combustion research is primarily focused on increasing the engine efficiency and reducing the emission products such as soot and nitrogen oxides (NO_x) [1]. One way to achieve low-emissions is to target at low-temperature and fuel-lean combustion conditions [2]. Combining the advantages of compression ignition (CI) and spark ignition (SI) engine systems, dual-fuel (DF) engines offer a promising solution to reduce particulate matter (PM) and NO_x emissions by providing low-temperature and fuel-lean combustion [3–5].

In DF engines, a high-reactivity fuel spray (e.g. diesel) is injected into a low-reactivity primary fuel (e.g. methane–air mixture) to release sufficient heat and chemically active reactants to ignite the ambient mixture under compression. Depending on various aspects, including the engine size, operation range and relative

ratio of the two fuels, such a fuel spray ignition scenario may differ substantially between different applications. For example, in reactivity controlled compression ignition (RCCI) engines, the two fuels are present commonly in energy-wise similar quantities, up to 70–90% low-reactivity fuel (LRF) ratio [6]. In the RCCI mode, the high-reactivity fuel is typically injected quite early before the top dead center (TDC), targeting towards a volumetric and staged ignition with substantial mixing time. In contrast, high-reactivity pilot spray may also be injected close to the TDC in rather small amounts (e.g. LRF ratio higher than 90%) [7], acting as a robust spark and eventually leading to combustion of the low-reactivity primary fuel. This paper focuses on continuous spray injection with high LRF ratio and close to TDC, which is common in industrial applications.

Due to the complexity of spray combustion, there is a need for comprehensive experimental data in order to better understand the associated fundamental physical and chemical phenomena. A number of datasets relevant to spray ignition at engine-relevant conditions exist for diesel and gasoline fuels in the Engine Combustion Network (ECN) database [8]. The main goal of the ECN

* Corresponding author.

E-mail address: bulut.tekgul@aalto.fi (B. Tekgül).

Table 1
Summary of recent key studies related to DF spray combustion and ignition characteristics.

Author	Configuration	Model	Added value	Ref.
Kahila et al. (2019a, 2019b)	<i>n</i> -dodecane DF spray	LES	Ignition characteristics and t_{inj} effect	[26,27]
Ahmad et al. (2019)	Diesel DF spray	Experiment	Pilot ratio and ϕ_{CH_4}	[46]
Srna et al. (2019a, 2019b)	<i>n</i> -dodecane DF spray	RCEM Exp. + OD	$T_{50\%}$, p_{inj} , t_{inj} , EGR effects and optical imaging	[35,36]
Grochowina et al. (2018)	Diesel DF combustion cell	Experiment	DF spray characteristics	[47]
Ghaderi Masouleh et al. (2017)	<i>n</i> -dodecane DF mixture	OD + 1D	Mechanism performance analysis	[48]
Demosthenous et al. (2016)	<i>n</i> -heptane DF spray	DNS	TCI + kinetics	[42]
Schlatter et al. (2016)	<i>n</i> -heptane DF spray	RCEM Exp. + OD	First detailed optical imaging	[34]

is to create well documented datasets suitable for numerical and experimental validation. Among different target conditions, the ECN Spray A is a suitable candidate for this study. It corresponds to a constant volume diesel spray combustion experimental setup, details of which are discussed in Section 2.4.

Previously, many experimental [9–13] and numerical [14–20] studies have been conducted investigating the Spray A configuration, all agreeing on the increase in IDT at lower ambient temperature conditions. In particular, Pei et al. [21–23] and Ameen et al. [24] concluded that lower ambient temperature levels lead to substantially higher IDT and leaner combustion characteristics due to longer mixing timescales. Moreover, Kundu et al. [25] reported the increase in influence of turbulent strain on chemistry in reacting flows at lower ambient temperatures. Following our previous work, here the ECN Spray A target condition is considered as a baseline case, enabling validation of the spray-LES framework [26,27].

Although there has been a growing interest in DF combustion research, so far results have mostly focused on the performance and emission characteristics of engine scale applications [28–33]. However, an agreement is reached on the retarding effect of ambient CH_4 on diesel spray ignition process through different studies. Rapid compression-expansion machine (RCEM) experiments conducted by Schlatter et al. [34] with *n*-heptane and ambient oxidizer containing CH_4 showed a linear relation between increase in IDT and the methane concentration of the ambient mixture. Following their work, Srna et al. [35,36] observed a similar behavior with *n*-dodecane and concluded that the retarding effect increases at lower temperatures and higher methane–air equivalence ratios. Almost all previous studies noted that there is an increase in the inhibiting effect of methane on IDT at lower temperatures for DF configurations. A large amount of numerical studies investigating DF combustion with diesel pilot ignition is also available in literature [3,4,37–44]. These studies range from OD models [45] to full scale 3D RANS simulations with finite-rate chemistry combustion modeling [3,4,37,39]. A summary of recent key studies investigating DF ignition is provided in Table 1.

While chemical oxidation process of diesel has been investigated from the chemistry point of view before, direct effect of CH_4 on this phenomenon is still ambiguous. Recently, Manias et al. [49] investigated the influence of CH_2O and H_2O_2 additives on CH_4 autoignition chemistry. Such species are known to be produced during the long hydrocarbon decomposition process and their presence is known to reduce the autoignition timescales considerably [26].

With relevance to the present paper, Kahila et al. [26,27] carried out high-resolution (62.5 μm) LES of DF spray ignition where *n*-dodecane was injected into a lean methane–air mixture in engine-relevant conditions at 900 K. The spray configuration corresponded to the ECN Spray A case, allowing extensive validation of the utilized numerical models against the available experimental data in SF configuration. The authors reported that the DF ignition is a volumetric process with three main stages: first-stage ignition and early heat release, second stage ignition at spray tip and activation of high-temperature chemistry and full oxidation

of available premixed low-reactivity fuel. It was observed that the DF IDT values are increased by a factor of 1.6–2.4 compared to SF at 900 K, depending on the applied chemical mechanism. In addition, it was reported that the ambient methane influences the *n*-dodecane ignition throughout the chemical oxidation process and inhibits both first and second-stage ignition, compared to the SF. In particular, the early decomposition of *n*-dodecane was reported to be inhibited by methane related reactions, hence supporting the findings of the longer first-stage IDT values observed by Srna et al. [50] in RCEM experiments. Finally, it was observed that the high-temperature ignition in LES appears in rich mixture, around $Z \approx 2Z_{st}$.

Based on the literature, several research gaps were identified to be addressed in this paper. First, suitability of the spray-LES framework for lower ambient oxidizer temperatures in spray combustion context has not been investigated. Second, in depth analysis of DF ignition characteristics with varying ambient temperature is yet to be analyzed in detail. Third, although the retarding effect of CH_4 to diesel spray ignition is known from engine and RCEM experiments, the trend as a function of ambient temperature is not fully quantified. Based on the noted research gaps, the following objectives are set for the paper:

1. Carry out simulations in OD, 1D and 3D to extend the work by Kahila et al. [26,27] on DF ignition for a range of temperatures.
2. Compare the effect of chemical mechanism in OD and 1D for an engine-relevant temperature range.
3. Perform 3D LES of SF and DF spray ignition at different temperatures (850, 900 and 1000 K).
4. Explain the inhibiting influence of methane on ignition at different ambient temperatures from mixing and chemical kinetics points of view.

The present paper is organized as follows: the numerical methods and utilized tools, such as governing equations, numerical discretization, turbulence and combustion models are presented in Sections 2.1 and 2.2, followed by a description of the different chemical mechanisms used and the simulation setup in Sections 2.3 and 2.4. Results obtained from OD, 1D and 3D simulations are presented in Section 3. In Section 4, an overall summary of the findings and the conclusion are presented.

2. Methodology

2.1. Governing equations and discretization

Gas phase fluid flow is governed by the compressible Navier–Stokes equations. In reactive flows, governing equations consist of continuity, momentum, species concentration and enthalpy. LES formulation of these equations with Favre-filtering is given as:

$$\frac{\partial \bar{\rho}}{\partial t} + \frac{\partial \bar{\rho} \tilde{u}_i}{\partial x_i} = \bar{S}_\rho, \quad (1)$$

$$\frac{\partial(\bar{\rho}\tilde{u}_i)}{\partial t} + \frac{\partial(\bar{\rho}\tilde{u}_i\tilde{u}_j)}{\partial x_j} = \frac{\partial}{\partial x_j}(-\bar{p}\delta_{ij} + \bar{\rho}\tilde{u}_i\tilde{u}_j - \bar{\rho}\tilde{u}_i\tilde{u}_j + \bar{\tau}_{ij}) + \bar{S}_{u,i}, \quad (2)$$

$$\frac{\partial(\bar{\rho}\tilde{Y}_k)}{\partial t} + \frac{\partial(\bar{\rho}\tilde{u}_i\tilde{Y}_k)}{\partial x_i} = \frac{\partial}{\partial x_i}\left(\bar{\rho}\tilde{u}_i\tilde{Y}_k - \bar{\rho}\tilde{u}_i\tilde{Y}_k + \bar{\rho}\tilde{D}\frac{\partial\tilde{Y}_k}{\partial x_i}\right) + \bar{S}_{Y_k} + \bar{\omega}_k, \quad (3)$$

$$\begin{aligned} \frac{\partial(\bar{\rho}\tilde{h}_t)}{\partial t} + \frac{\partial(\bar{\rho}\tilde{u}_j\tilde{h}_t)}{\partial x_j} \\ = \frac{\partial\bar{p}}{\partial t} + \frac{\partial}{\partial x_j}\left(\bar{\rho}\tilde{u}_j\tilde{h}_t - \bar{\rho}\tilde{u}_j\tilde{h}_t + \frac{\bar{\lambda}}{c_p}\frac{\partial\tilde{h}_t}{\partial x_j}\right) + \bar{S}_h + \bar{\omega}_h, \end{aligned} \quad (4)$$

where $\bar{\rho}$, \tilde{u}_i , \bar{p} , \tilde{Y}_k , \tilde{h}_t , $\bar{\tau}_{ij}$ represents filtered density, velocity, pressure, mass fraction of k^{th} species, sensible enthalpy and viscous stress tensor, respectively. In this notation, overbar ($\bar{}$) denotes unweighted ensemble average and tilde ($\tilde{}$) denotes density-weighted ensemble average. In energy equation (i.e. Eq. (4)), variables \bar{c}_p and $\bar{\lambda}$ represent heat capacity and thermal conductivity of the mixture. In reacting cases, production rate of each specie is denoted by $\bar{\omega}_k$ and heat release rate (HRR) is calculated as $\bar{\omega}_h = \sum_k \Delta h_{f,k}^o \bar{\omega}_k$, where $h_{f,k}^o$ is the enthalpy of formation. A unity Lewis number is assumed for all the species, making the diffusion coefficient $D = \lambda/(\rho c_p)$. The system of equations is completed by the ideal gas law and thermal equation of state.

Finite volume method is utilized to solve Eqs. (1)–(4) with a 2nd order implicit time integration method within OpenFOAM-2.4.x framework [51]. The reacting PISO (Pressure-Implicit with Splitting of Operators) algorithm is utilized to achieve pressure-velocity coupling. While diffusion terms are discretized by 2nd order central differencing schemes, convection related terms required a different discretization strategy due to their non-linearity and subgrid scale modeling. The LES subgrid parameters present in the Eqs. (1)–(4) can be explicitly modeled through a subgrid scale turbulence model. Alternatively, with a suitable grid size, they can also be implicitly modeled by choosing a dissipative numerical discretization scheme for convection terms. In this work, the latter path is taken with utilizing a non-linear, dissipative interpolation scheme called Gamma scheme [52] for scalar and convective term discretizations, which is similar to our previous studies involving non-reactive and reactive spray simulations [19,26,27,53].

2.2. Spray and combustion modeling

For modeling the injected liquid diesel surrogate spray, Lagrangian Particle Tracking (LPT) method is used, similar to our previous spray simulation studies [19,26,27,53]. The initial particles are sampled as computational parcels using Rosin-Rammler distribution with an initial Sauter mean diameter of 6 μm . The secondary break-up of the droplets is modeled using the KHRT model [54,55]. Frössling correlation [56] and Ranz and Marshall correlation [57,58] are used to model the evaporation between the two phases.

The reactivity is introduced to the governing equations through source terms in Eqs. (3) and (4): filtered species reaction rates ($\bar{\omega}_k$) and heat release rate (HRR) ($\bar{\omega}_h$). Due to the large timescale difference between the flow and the chemistry, an operator-splitting technique is used to split the calculation of gas phase flow equations from chemical source term calculation step.

In our OpenFOAM implementation, calculation of the Jacobian matrix for solving the chemical source term ODE system is carried out with the open-source library pyjac [59]. The stiff ODE system is

solved independently for each computational cell, using a linearly implicit Euler extrapolation method (Seulex) [60] with high-order (up to 12th) accuracy. Finally, the computational load of the chemistry calculation is optimized through MPI routines and uniformly distributed to the available processors during simulation.

The turbulence-chemistry interaction (TCI) is taken into account through a first order closure hypothesis and no subgrid scale model is applied for the chemical source terms in Eqs. (3) and (4). Similar to our previous study, it is assumed that the turbulence levels in the high velocity spray leads to such an intense mixing, that with the present mesh resolution finite-rate chemistry is able to predict the ignition characteristics sufficiently [26]. Previously, Pei et al. [21] utilized a similar first order approach in Spray A using a similar grid spacing to the present study and reported reasonable results. In addition, LES studies in configurations including non-premixed and premixed combustion modes have shown promising results with such a simplified no-model approach [61–63]. In general, adequate performance of this simple approach is attributed to the comparatively fine grid resolutions used in the prescribed studies. However, it has been shown earlier that the influence of strain effects and mixing on reactive sprays (e.g. modeling uncertainties) increase at lower ambient temperature conditions [25]. In general, it should be noted that the current TCI approach introduces a modeling error to the simulation. However, according to our previous investigations [26,27] and compiled results in the recent ECN proceedings [64], the TCI model has less influence on IDT compared to dynamics of e.g. transient spray flame stabilization phenomenon.

Finally, the chemistry computation is further optimized by computing the full detailed chemistry solution only within the spray region ($Z > 1e-4$). Elsewhere, where homogeneous premixed methane mixture is present ($Z < 1e-4$), chemistry solution is integrated for a single cell and mapped to other cells. This provides significant computational speedup especially at the beginning of the simulation, where the fuel spray is spatially confined.

2.3. Chemical mechanisms

Choosing a suitable chemical mechanism plays a crucial role in reactive simulations. There are various mechanisms governing the *n*-dodecane oxidation process. However, the chosen mechanism should also properly predict CH_4 oxidation and the effect of CH_4 on *n*-dodecane oxidation.

At lower ambient temperature conditions, contribution of the low-temperature combustion (LTC) and related reactions to overall oxidation path increases. The ECN workshops reported that the chemical mechanisms carry much significance for modeling LTC accurately [64]. Wehrfritz et al. [65] showed that for low temperature conditions around 750–800K, differences in ignition delay can be as high as 2 ms for different chemical mechanisms at the Spray A (SF) conditions. In a different study by Ghaderi Masouleh et al. [48], various *n*-dodecane mechanisms by Sarathy et al. [66], Ranzi et al. [67,68], Narayanaswamy et al. [69] and Luo et al. [70] were investigated in 0D and 1D DF modeling context and their performance on ignition modeling was explored. However, most of these mechanisms are considered too large to be used in 3D LES simulations.

In our previous study, Kahila et al. [26] have shown that the compact skeletal mechanism developed by Yao et al. [71] (hereby referred to as Yao) and another reduced mechanism developed by Frassoldati et al. (hereby referred to as POLIMI reduced) [72] were able to reproduce similar features during the DF oxidation process, including the interactions between CH_3 , OH and long hydrocarbon radicals, relevant to CH_4 and *n*-dodecane oxidation. Consistent with that study, the main chemical mechanism utilized in this study is the compact Yao mechanism. For completeness, we

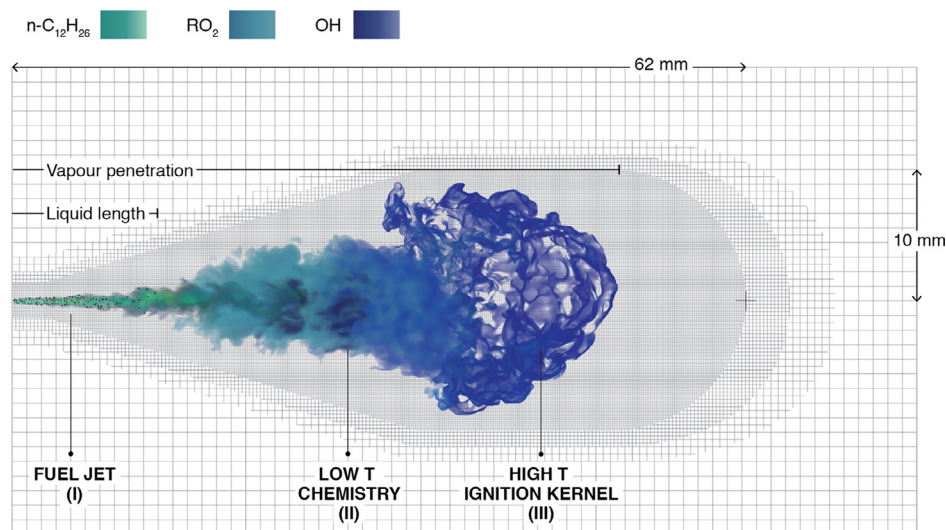


Fig. 1. Volume rendering of the LES data for DF 900 K case. Non-reacting fuel jet ($n\text{-C}_{12}\text{H}_{26}$, green), LTC (RO_2 , transition region), and high temperature ignition kernel (OH, blue) are represented. (For interpretation of the references to color in this figure legend, the reader is referred to the web version of this article.)

Table 2
Chemical mechanisms for n -dodecane oxidation.

Mechanism name	Species	Reactions	Reference
Yao	54	269	[71]
Polimi reduced	96	993	[72]
LLNL reduced	163	887	[73]
Narayanaswamy	255	1512	[69]

provide a mechanism comparison in 0D and 1D simulations with two additional mechanisms from Lu et al. [73] (referred as LLNL reduced) and Narayanaswamy et al. [69] (referred to as Narayanaswamy). From these mechanisms, POLIMI reduced was analyzed in a comparative study investigating n -dodecane/ CH_4 blends with homogeneous reactor simulations [48], while Yao and LLNL reduced were validated against experimental RCEM data [74]. Narayanaswamy was included in both of these studies. These results combined with our previous spray modeling studies using flamelet models [19,53] and finite-rate chemistry [26,27] show that all the selected mechanisms are able to describe n -dodecane oxidation kinetics consistently. It is also important to note that all the mechanisms except POLIMI reduced were reduced from the same detailed mechanism developed by Sarathy et al. [66]. A brief summary of the chemical mechanisms considered is provided in Table 2.

2.4. Simulation configuration and case setup

The numerical SF spray analysis conducted in this study corresponds to the ECN Spray A conditions [8]. Diesel fuel surrogate n -dodecane is injected from a $90\ \mu\text{m}$ nozzle orifice into a constant volume combustion vessel, where the thermophysical properties are similar to engine conditions. There is an extensive additional data for different ambient temperature conditions, ranging from 750 to 1200 K. The corresponding DF setup derived from the baseline Spray A condition has additional CH_4 in the ambient mixture, which is achieved by keeping the molar concentration of O_2 constant and adding CH_4 to the ambient mixture until $\phi_{\text{CH}_4} = 0.5$ condition is satisfied. Based on these conditions, stoichiometric mixture fraction (Z_{st}) corresponds to $Z_{st}^{\text{SF}} = 0.0435$ and $Z_{st}^{\text{DF}} = 0.0234$ for SF and DF cases. Details of this experimental setup and the DF condition derived from it is given in Table 3.

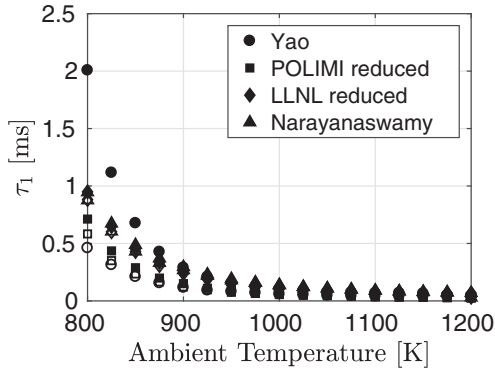
Table 3
Spray case details and computational setup.

	ECN Spray A	DF Spray A
Inj. parameters		
Fuel	$n\text{-C}_{12}\text{H}_{26}$	$n\text{-C}_{12}\text{H}_{26}$
Nominal nozzle diameter, D	$90\ \mu\text{m}$	$90\ \mu\text{m}$
Fuel temperature	363 K	363 K
Injection pressure	150 MPa	150 MPa
Injection duration	Continuous	Continuous
Ambient conditions		
Temperature	800–1200 K	800–1200 K
Density	$22.8\ \text{K/m}^4$	$22.8\ \text{K/m}^4$
X_{O_2}	0.15	0.15
X_{CO_2}	0.0623	0.05955
$X_{\text{H}_2\text{O}}$	0.0362	0.0346
X_{N_2}	0.7515	0.71835
X_{CH_4}	0	0.0375
ϕ_{CH_4}	0	0.5

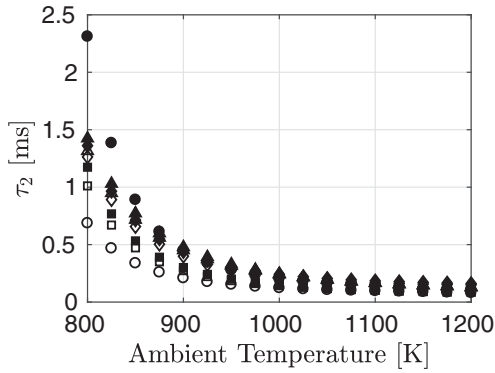
For 3D LES analysis, the computational domain is constructed to have the same volume with the experimental combustion vessel [8]. The simulation setup is depicted in Fig. 1. A refinement region of $62.5\ \mu\text{m}$ is applied around the region where n -dodecane spray penetrates. This grid resolution has been shown to be fine enough to capture important spray features in previous numerical studies [16,18,19,21,24–27,53]. For all cases, spray penetration is included within the prescribed uniform resolution. In zone (I), strong momentum exchange, mixing, and liquid evaporation take place. In the present LES-LPT model, the spatial dimensions of zone (I) depend mostly on droplet size (via the Stokes number), fuel thermo-physical properties (e.g. latent heat) and injection conditions (e.g. injection pressure, duration, and nozzle diameter). Towards the end of zone (I) and in the LTC zone (II), low-temperature reactions occur. The LTC zone (II) terminates at the point where high temperature reactions start at the border of high-temperature combustion (HTC) zone (III). Finally, the HTC zone expands towards the ambient CH_4 -air mixture. Based on previous studies, the inhibiting effect of ambient CH_4 to diesel spray ignition mostly occurs between the zones (I) and (II), affecting the early stage LTC [26,35,36].

3. Results

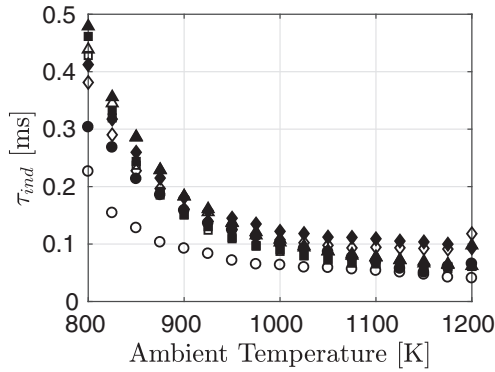
In order to understand the different physical and chemical phenomena affecting ignition in reactive dual-fuel sprays, nu-



(a) First stage IDT's (τ_1)



(b) Second stage IDT's (τ_2)



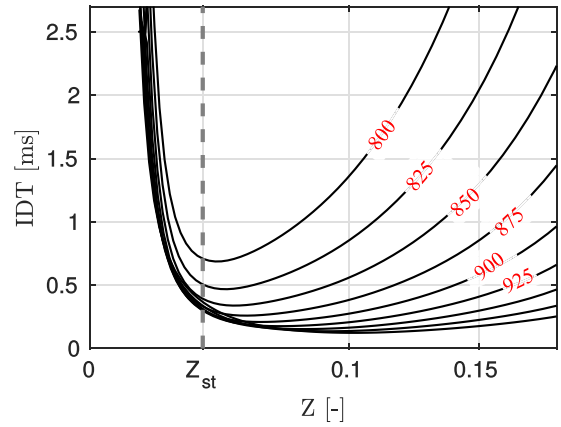
(c) Chemical induction time ($\tau_2 - \tau_1$)

Fig. 2. IDT results obtained from most reactive mixture fraction (Z_{MR}) value of homogeneous reactors set along the adiabatic mixing line at 800–1200 K ambient temperature range (SF – open, DF – filled symbols).

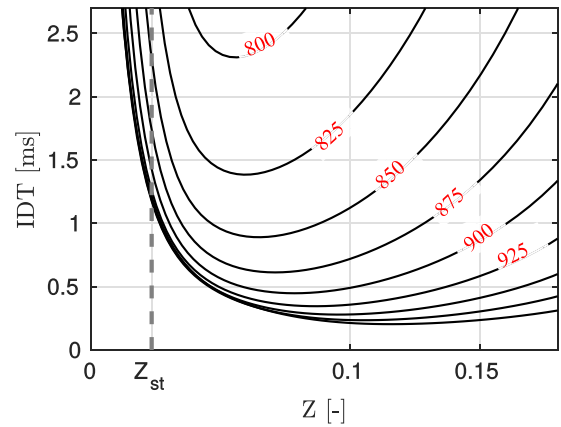
merical simulations are presented in this section in an order based on their level of complexity: 0D homogeneous reactor (HR) simulations, 1D counter-flow diffusion flamelet (CDF) simulations and 3D LES spray simulations.

3.1. Homogeneous reactor simulations (0D)

Constant pressure HR simulations are carried out using the Cantera software [75]. In particular, we compare four different *n*-dodecane reaction mechanisms and investigate SF and DF IDT's along the adiabatic mixing line. We note that the concept of the



(a) SF



(b) DF

Fig. 3. IDT values of 0D homogeneous reactors set along the adiabatic mixing line for a range of ambient temperatures using Yao mechanism.

adiabatic mixing line has particular relevance in spray-originated non-premixed combustion.

IDT values for both SF and DF conditions are obtained and presented in Fig. 2(a). First stage IDT (τ_1) is the characteristic time of LTC onset and here it is defined as the time instance when 20% of maximum $C_{12}H_{25}O_2(RO_2)$ concentration ($Y_{RO_2})_{max}$ is reached. Second stage IDT (τ_2), or the high temperature ignition, represents the full ignition of the mixture and initiation of high-temperature chemistry (HTC). The definition of τ_2 is based on the maximum value of the maximum temperature gradient $(\frac{dT_{max}}{dt})_{max}$. While Fig. 2(a) and (b) show τ_1 and τ_2 of the SF and DF mixtures, Fig. 2(c) presents the chemical induction time ($\tau_{ind} = \tau_2 - \tau_1$) for all cases.

From Fig. 2, the following observations can be made: (1) Lower ambient temperature indicates higher τ_1 and τ_2 values for both SF and DF configurations. (2) The inhibiting effect of methane on τ_1 and τ_2 is observed for all four mechanisms and the effect increases with decreasing temperature. (3) For $T \geq 950$ K, τ_{ind} values are found to be independent of temperature and methane addition (SF vs. DF). However, at $T < 950$ K, τ_{ind} becomes substantially more dependent on temperature and methane addition. (4) While the τ_2^{DF}/τ_2^{SF} ratio (not shown in figure) is between 1.2 to 1.4 for three of the selected mechanisms at different ambient temperatures, the Yao mechanism yields a higher ratio in the range of 1.4 to 3.4. Qualitatively, these findings are consistent with the results by Srna et al. [35,36], where the inhibiting effect of methane was

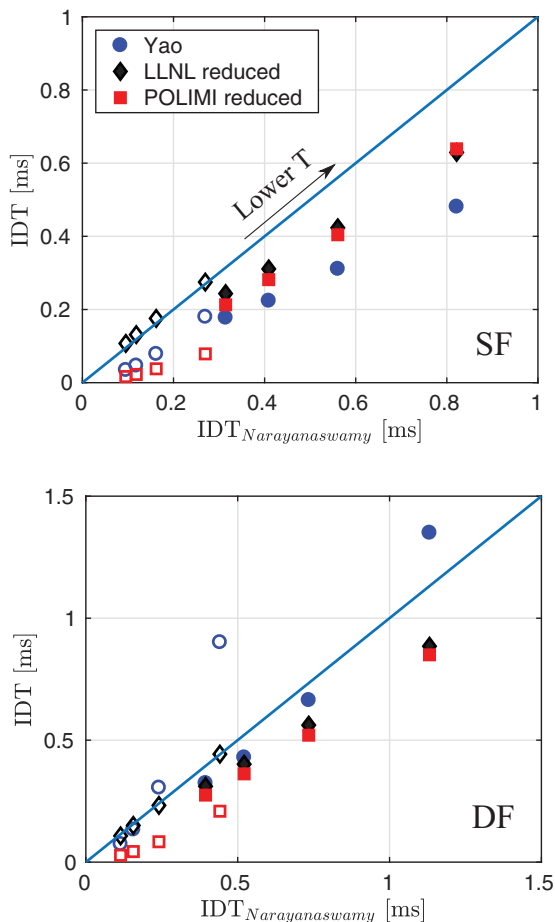


Fig. 4. Comparison of IDT results obtained from 1D flamelet simulations for 850–1000 K range (SF-left, DF-right). Narayanaswamy mechanism is taken as the comparison baseline since it is the largest one among the investigated mechanisms. Open markers represent τ_1 while filled markers represent τ_2 .

found to increase at lower temperatures, and the retarding effect of methane was reported to diminish after the initiation of LTC.

Overall, Fig. 2 shows an increasing discrepancy in IDT with decreasing temperature. In particular, the Yao mechanism seems to produce longer IDT values at Z_{MR} compared to the other mechanisms. Due to high complexity of chemical kinetics at low temperatures and within the negative temperature coefficient (NTC) region, such deviations are expected [76]. For example, Yao et al. [71] show high sensitivity to low-temperature reactions on Spray A IDT at 800 K. Therefore, compared to other mechanisms, a certain over-prediction of the ignition events by the Yao mechanism at lower temperatures is anticipated for both SF and DF.

The IDT's calculated along the adiabatic mixing line with the Yao mechanism are presented in Fig. 3. It can be seen that at low temperatures, the igniting mixtures are more confined in the mixture fraction domain in DF cases. Such a confining behavior is due to the effect of added methane: in DF conditions the retarding effect creates a narrower band of mixture fraction values active enough to ignite within a relevant time frame, which in turn delays the IDT. Increasing the ambient temperature diminishes this effect and the SF and DF cases show similar behavior for the higher temperature conditions.

3.2. Counter-flow diffusion flamelets (1D)

Next, 1D igniting counter-diffusion flamelet (CDF) simulation results are presented to investigate the joint effect of laminar

mixing and diffusion on ignition chemistry characteristics. The governing equations for the transient CDF [77,78] are solved using the Chem1D software [79]. The initial and boundary conditions of the flamelets are set according to Table 3 with a unity Lewis number assumption. Here, a constant strain rate of 500 s^{-1} is used, a value shown previously to capture the moderately strained conditions [19,26,53].

Figure 4 provides a quantitative comparison of the mechanisms for the 1D simulations. Narayanaswamy is selected as the baseline reference since it is the most detailed among the investigated mechanisms. It can be seen that for the baseline SF condition, Yao tends to underpredict both τ_1 and τ_2 . In the DF configuration, Yao overpredicts both τ_1 and τ_2 compared to the reference at higher IDT values, corresponding to lower temperature conditions. However, the overall performance of the selected mechanisms seem to be following the same trend. Considering the compactness and overall performance above the desired lower temperature limit (850K), the Yao mechanism is chosen to be used for 3D simulations. Therefore, the following 1D flamelet analysis is limited to the results obtained with the Yao mechanism.

We have already investigated the ignition characteristics of 1D SF and DF laminar flamelets at 900 K in our previous work [26]. Utilizing a similar analysis, three characteristic time instances associated with ignition process are computed for each case in mixture fraction-time (Z, t) space and the results are presented in Fig. 5. For brevity, two conditions corresponding to the lower and higher limits of our focus ambient temperature range (850 and 1000 K) are given. Numerical results for all investigated cases are presented in Table 4. The obtained results follow the same trends as the 0D homogeneous reactor simulations at different temperatures which are provided in the supplementary materials of the paper.

The timescale τ_1 (●) is defined similar to before as the time instance when 20% of $(Y_{\text{RO}_2})_{\text{max}}$ is reached. It is associated with LTC and its position in (Z, t) space corresponds to the onset of early heat release at low mixture fraction conditions. It can be seen from Fig. 5 that CH_4 addition shifts the LTC initiation to richer mixture fraction conditions, which is consistent with the 0D results. From Table 5 it can also be observed that τ_1 increases with CH_4 addition and the effect is the strongest at lower ambient temperatures (increase around 0.9 ms for 850 K).

After a sufficient time, the HTC is activated and the mixture progresses to higher burning temperatures. Second timescale, the τ_{HTC} (■) is defined as the time instance when 1% of maximum H_2O_2 consumption rate is reached [80] and similar to LTC, a shift to the richer mixtures due to CH_4 addition can be observed. It is noted that the addition of CH_4 not only delays τ_1 , but also τ_{HTC} . However, the induction time between these two time instances ($\tau_{\text{HTC}} - \tau_1$) seems to be unaffected by CH_4 , further supporting the view that the timescales after τ_1 seem to be only weakly dependent on ϕ_{CH_4} (SF vs. DF).

After the HTC onset, there is another characteristic timescale until high-temperature oxidation progresses. This stage is defined similar to the second-stage ignition introduced previously and denoted as τ_2 (▲). It is defined as the time instance when maximum value of temperature gradient $(\frac{dT}{dt})_{\text{max}}$ is obtained. Typical to diesel ignition process, after HTC onset, HTC drifts towards leaner mixtures. From Table 5 it can be seen that the induction time between τ_2 and τ_{HTC} increases with lower ambient temperature for both SF and DF conditions. It is also evident that CH_4 addition increases this time interval by around 0.1 ms, with weak ambient temperature dependency. A similar observation can be made for the overall induction time between the two main ignition events ($\tau_2 - \tau_1$). Although the independent inhibiting effect of CH_4 and

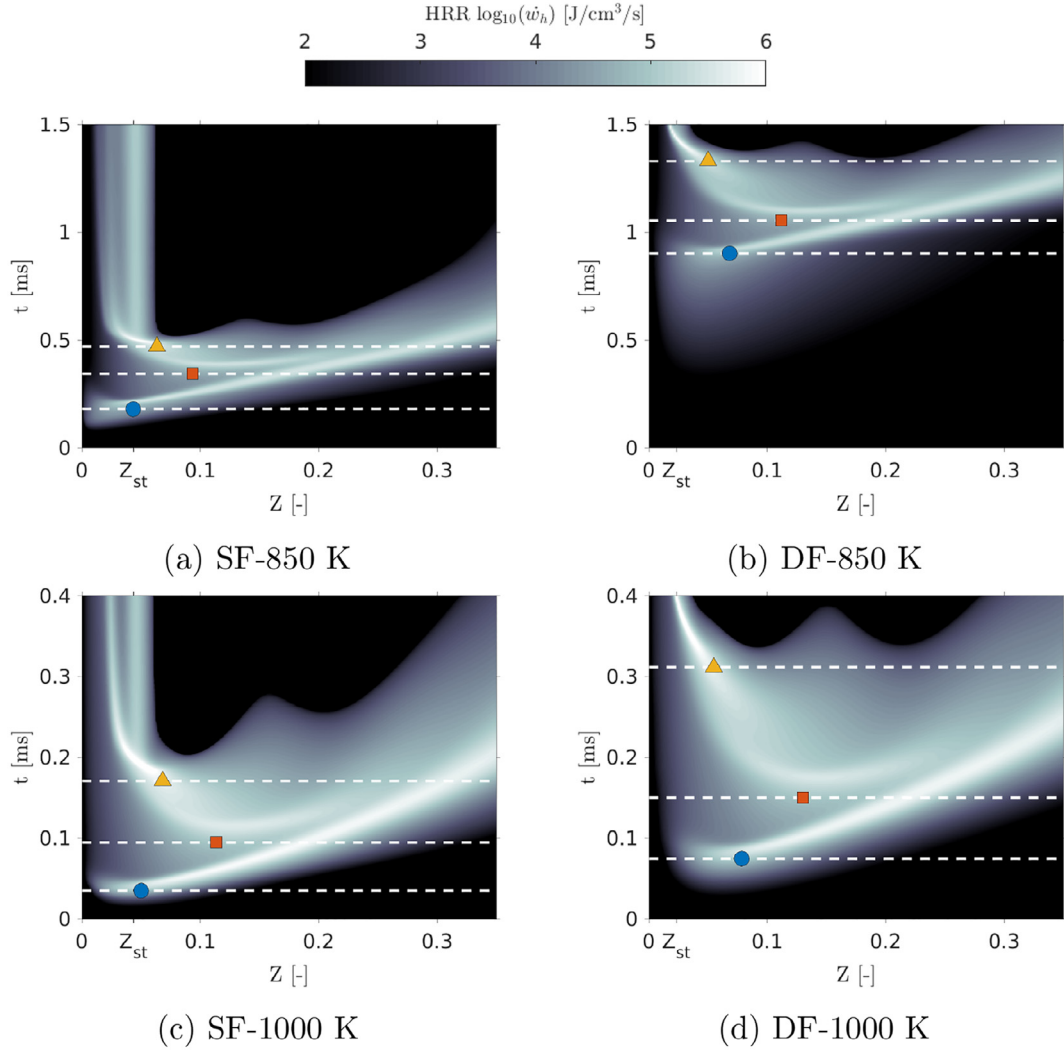


Fig. 5. HRR of 1D flamelets in Zt space for SF (a,c) and DF (b,d) cases. Markers denote the time instances where: τ_1 (●) 20% of $(Y_{\text{RO}_2})_{\text{max}}$ is reached, τ_{HTC} (■) 1% of $(\dot{\omega}_{\text{H}_2\text{O}_2})_{\text{min}}$ is reached and finally τ_2 (▲) time at maximum temperature gradient $(\frac{dT_{\text{max}}}{dt})_{\text{max}}$ is obtained. Note the change in y-axis limits between 850 and 1000 K.

Table 4

Characteristic ignition time instances presented in Fig. 5 and the time difference between them. While the overall inhibition of all characteristic timescales with lower temperatures and CH_4 addition is evident, the characteristic time $(\tau_{\text{HTC}} - \tau_1)$ seems to be insensitive to the CH_4 addition.

	τ_1 [ms] (●)	τ_{HTC} [ms] (■)	τ_2 [ms] (▲)	$(\tau_{\text{HTC}} - \tau_1)$	$(\tau_2 - \tau_{\text{HTC}})$	$(\tau_2 - \tau_1)$
SF						
850 K	0.1802	0.3438	0.4704	0.1636	0.1266	0.2902
900 K	0.07876	0.2013	0.3023	0.12254	0.101	0.22354
1000 K	0.03479	0.09457	0.1707	0.05978	0.07613	0.13591
DF						
850 K	0.9019	1.054	1.33	0.1521	0.276	0.4281
900 K	0.3056	0.4288	0.6483	0.1232	0.2195	0.3427
1000 K	0.0743	0.1498	0.3115	0.0755	0.1617	0.2372

lower temperature is visible, the inhibiting effect of CH_4 does not seem to increase much at lower temperature conditions.

Based on the 1D analysis, we conclude that: (1) The addition of CH_4 shifts the whole ignition process to richer mixture fraction conditions. (2) The time difference between τ_1 and HTC onset (τ_{HTC}) is unaffected by CH_4 addition, supporting the observation that CH_4 mainly inhibits the early oxidation process. (3) At any given temperature, the time difference between τ_2 and τ_1 seems to increase with methane addition (by 0.1–0.12 ms). Overall, the

flamelet simulations support the previous observations that the inhibiting effect of CH_4 on long hydrocarbon oxidation occurs mainly at the early stages of oxidation.

3.3. Large-eddy simulation of spray ignition (3D)

Next, SF and DF sprays are simulated at $T = 850, 900$ and 1000 K. On one hand, the chosen temperature range is justified based on the obtained 0D and 1D results which indicated temper-

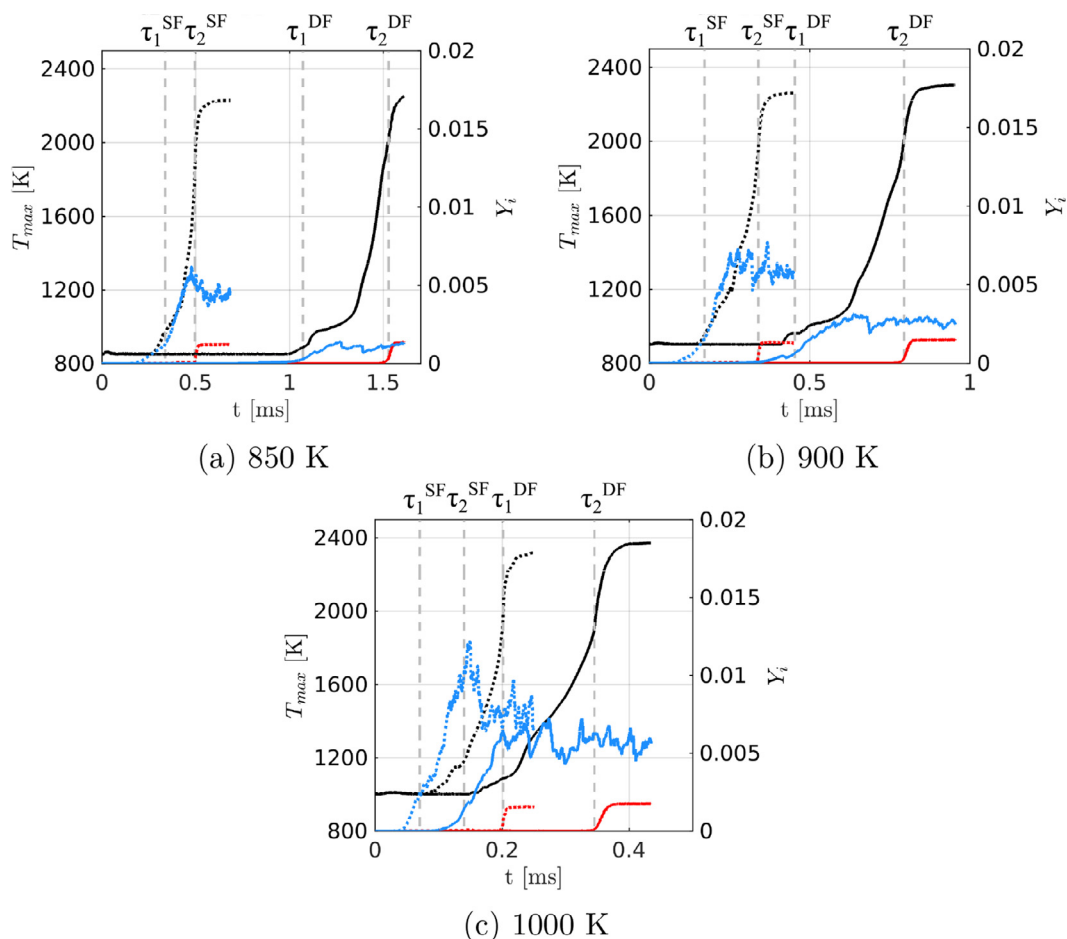


Fig. 6. Evolution of RO_{2max} (—), T_{max} (—) and OH_{max} (—) with respect to time. Dashed line represent SF while solid line shows DF. Note the change in horizontal axis scale for each case.

ature sensitivity for the Yao mechanism below 850 K. On the other hand, above 1000 K, the retarding effect of CH_4 is observed to diminish, making the higher temperature values of less interest. We note that the current baseline ECN Spray A simulation setup has been thoroughly validated in non-reacting ($Y_{O_2}=0$) conditions by comparing the vapor and liquid penetration and mixture profiles with the experimental results [16,19,53]. Additionally, the utilized solver has been benchmarked for various reacting configurations [26,27].

3.3.1. IDT definition and spatio-temporal DF ignition analysis

Figure 6 shows the temporal evolution of the maximum temperature in the 3D domain, along with concentrations of key species related to ignition for different ambient temperatures. The first and second stage IDT values (τ_1 and τ_2) are marked as vertical dashed lines in the figure. The temporal shift in T_{max} from SF (---) to DF (—) is evident for all temperature levels. In addition, the two-stage ignition structure associated with long hydrocarbon fuels can be clearly observed from the T_{max} curves.

In order to compare the ignition characteristics at different conditions in detail, IDT values are presented in Fig. 7 along with experimental Spray A IDT results for τ_2 . The SF Spray A IDT values obtained from LES (blue bar) show good agreement with the experimental data with a slight underprediction, which is expected for the Yao mechanism [74]. Furthermore, the retarded ignition for DF case is also clearly visible in the figure for both τ_1 and τ_2 . For lower ambient temperatures, the retarding effect of CH_4 increases. In addition, τ_2^{DF}/τ_2^{SF} is found to be 3.1 (850 K), 2.33 (900 K) and 1.71 (1000 K). Finally, relative insensitivity of τ_{ind}

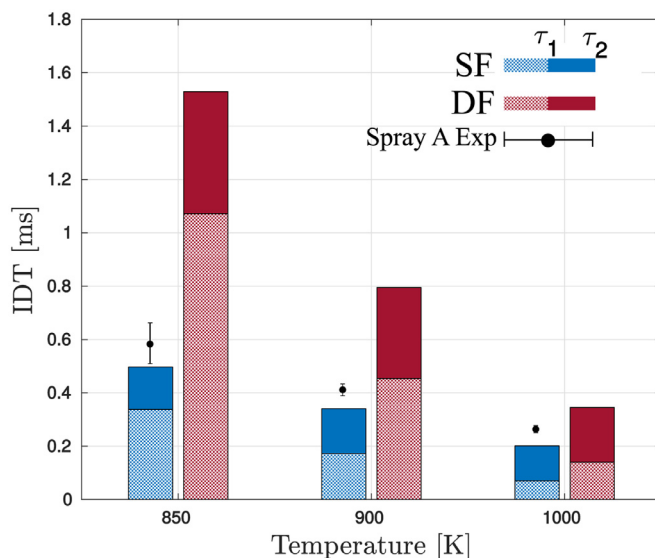


Fig. 7. IDT's of SF and DF cases obtained from 3D LES analysis. Patterned portion of the bar represents τ_1 while the total bar represents τ_2 . Inhibiting effect of CH_4 to both ignition stages is clearly observed. (For interpretation of the references to color in this figure, the reader is referred to the web version of this article.)

to ambient temperature can also be observed from Fig. 7. Such a characteristic behavior also supports the view that the CH_4 mostly

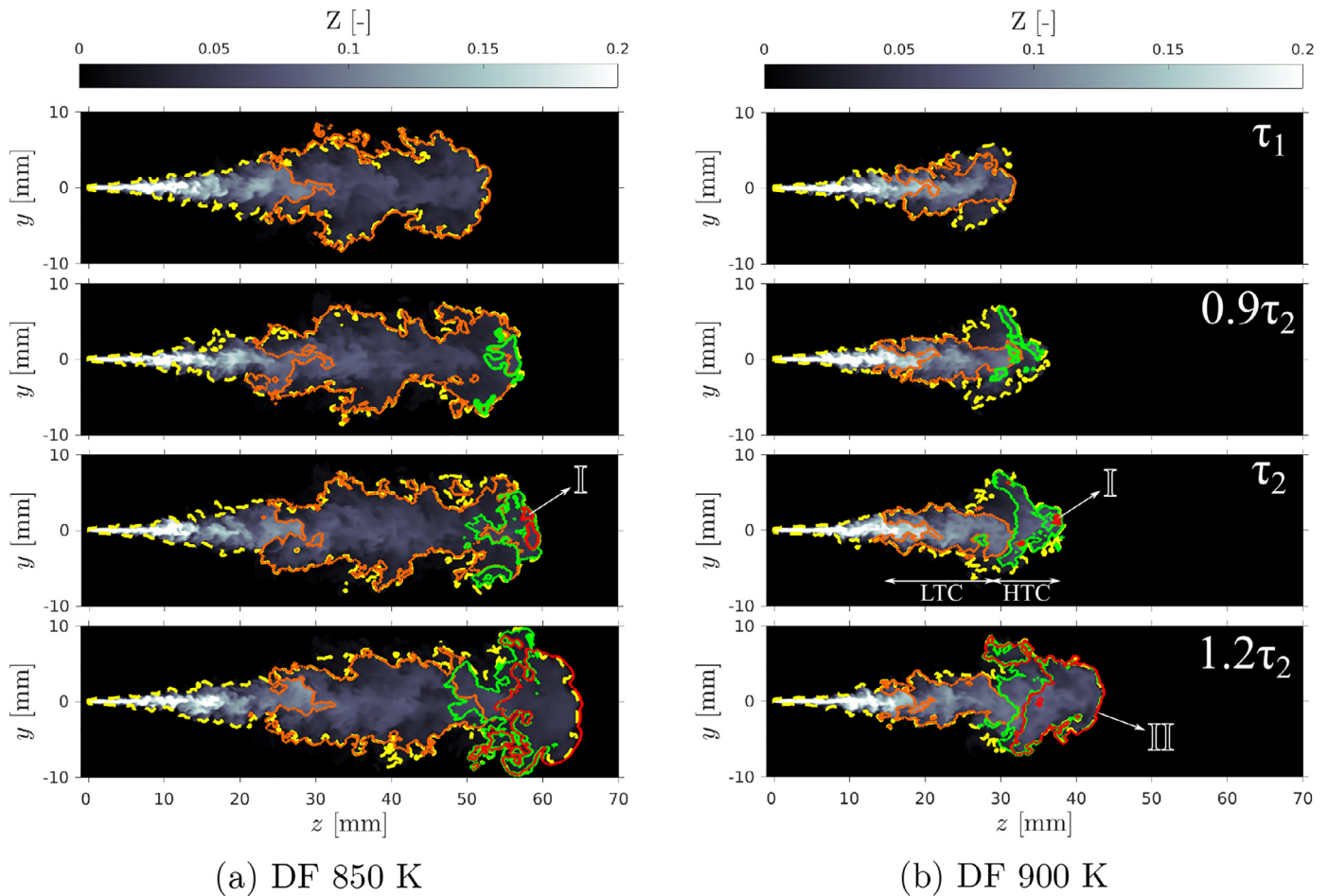


Fig. 8. Ignition process for different temperatures at DF configuration. Regions where LTC is taking place is represented with (—) while high-temperature chemistry is denoted by (—). Initial ignition kernels leading to flame front are marked with (—). Finally, stoichiometric mixture fraction Z_{st} is represented with dashed yellow line (—). (For interpretation of the references to color in this figure legend, the reader is referred to the web version of this article.)

retards the low-temperature reactions and causes a primary delay in the early oxidation products [26].

In order to understand the effect of ambient temperature on DF ignition, spatio-temporal species distribution is investigated and linked with the timescales τ_1 and τ_2 . Cutplane data from the DF spray simulations from different time instances is presented in Fig. 8 for 850 K and 900 K, while the 1000 K case is not shown for brevity. The chosen time instances are: (1) first stage ignition (τ_1) when LTC is initiated, (2) slightly before the second stage ignition ($0.9\tau_2$) when low and high temperature regions can be observed, (3) second stage ignition (τ_2) when first ignition kernels can be spotted, (4) slightly after the second stage ignition ($1.2\tau_2$) at the onset of ambient CH_4 consumption.

At $t = \tau_1$, first row of Fig. 8 shows the distribution of LTC (—) across the spray. The boundary of the LTC region is marked by the isoline of 1% of maximum of early oxidation products ($1\% (Y_{\text{RO}_2})_{\text{max}}$). At 850 K, τ_1 is higher, enabling longer mixing time and consequently a more diluted diesel spray. Such enhanced mixing can be observed in the LTC region, which is more confined towards richer regions at 900 K, whereas at 850 K LTC region leans out and follows more closely the stoichiometric mixture fraction Z_{st} (—) isoline. Additionally, the retarding effect of CH_4 on ignition can be seen from the onset of the LTC region from the nozzle. While at 850 K LTC initiates around 25 mm, at 900 K it shifts to 15 mm.

On the second row ($t = 0.9\tau_2$), growth of the LTC region throughout the spray can be observed. It is worth noting that the wider distribution of the LTC at lower temperatures is still visible.

In addition, onset of HTC (—) is also visible during this phase. The border of this region is marked by the isoline representing 1% of maximum H_2O_2 consumption rate ($1\% (\dot{\omega}_{\text{H}_2\text{O}_2})_{\text{min}}$), denoting the consumption of LTC phase products and eventually leading to HTC.

The third row ($t = \tau_2$) shows the second stage ignition for both cases. LTC and HTC structures can be easily identified and the formation of the first high temperature ignition kernels (—) is visible (I). This region is defined by the $T=1500$ K isoline and will eventually ignite the ambient CH_4 in the spray vicinity. It is clear that the ratio of LTC/HTC is much higher at 850 K, showing that LTC contribution to the heat release is higher than at 900 K. Finally, the last row ($t = 1.2\tau_2$) shows the growing HTC region (II), reacting with the ambient methane. This region follows the stoichiometric isoline covering the periphery of the spray tip for both temperatures. In addition to the reported results here, a spatial distribution analysis of formaldehyde (CH_2O) is provided as supplementary material to this paper to give more insight on the LTC characteristics in the investigated configurations.

A summary of the quantitative results for the 3D SF and DF sprays is provided in Table 5. The observed trends can be also understood in light of certain previous studies. First, Dahm et al. [81] have shown that the early conversion rate of n -dodecane is highly dependent on temperature, leading to slow increase in temperature and radical/intermediate species concentrations, prolonging τ_1 . Second, as discussed earlier by Kahila et al. [26], the early CH_4 related kinetics consumes important radicals such as OH, subsequently enhancing the inhibiting effect on the early

Table 5

First (τ_1), second stage (τ_2) ignition, chemical induction time ($\tau_{ind} = \tau_2 - \tau_1$), mean and standard deviation of HTC location (X_{HTC}) and liquid penetration (X_{liq}) for investigated LES cases.

	τ_1 [ms]	τ_2 [ms]	τ_{ind} [ms]	X_{HTC} [mm]	X_{liq} [mm]
SF					
850 K	0.37	0.5	0.13	27.0 ± 3.2	10.7 ± 2.13
900 K	0.19	0.34	0.15	21.3 ± 2.1	9.01 ± 1.65
1000 K	0.08	0.2	0.12	18.1 ± 2.0	8.92 ± 1.99
DF					
850 K	1.21	1.5	0.29	56.2 ± 2.1	11.69 ± 1.25
900 K	0.51	0.76	0.25	32.9 ± 2.5	10.22 ± 1.76
1000 K	0.16	0.35	0.20	22.5 ± 2.2	8.94 ± 2.04

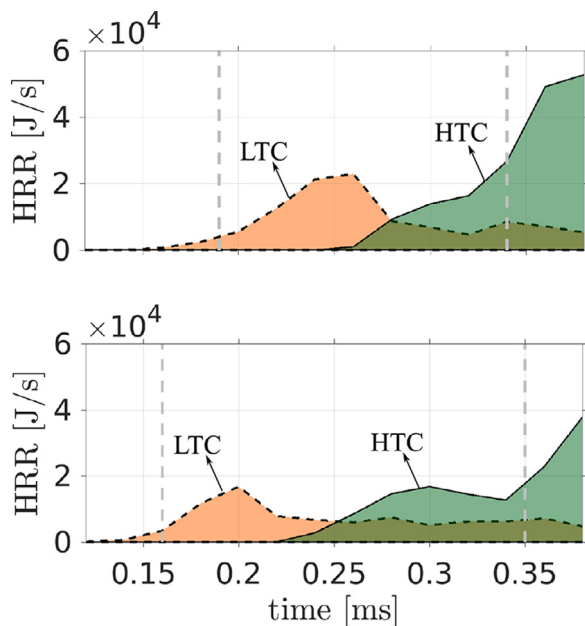


Fig. 9. Contribution of LTC and HTC stages to the heat release rate for SF 900 K (top) and DF 1000 K (bottom) conditions. Similar temporal evolution of LTC and HTC is observed for both cases.

n-dodecane decomposition. Therefore, inhibition of τ_1 at lower temperatures and in the presence of ambient CH_4 is expected. As shown earlier, τ_{ind} is less sensitive to temperature. After τ_1 , the accumulation of heat and radicals in the system reduces the inhibiting effect of CH_4 on the oxidation process, relative to conditions prior to τ_1 . In general, the LTC related reactions are expected to be more sensitive to temperature than the ones in HTC [80], which is also depicted in the Yao mechanism by high/low-temperature exponents for LTC/HTC reactions [71].

In addition to the above, according to Table 5, conditional mean of the HTC location (X_{HTC}) away from the nozzle tends to increase with lower temperature and CH_4 addition, consistent with the inhibiting effect of low ambient temperature and CH_4 to ignition. Finally, the average liquid penetration (X_{liq}) calculated for *n*-dodecane shows that while the liquid penetration increases with lower temperatures and CH_4 addition, the increasing effect of CH_4 on X_{HTC} diminishes between SF and DF cases at 1000 K. In contrast, at 850 K the DF spray ignites approximately by a factor of 2 longer distance than the SF spray.

3.3.2. Comparison of SF-DF ignition at similar IDT timescales

From Table 5, it can be seen that SF 900 K and DF 1000 K cases have τ_1 and τ_2 values close to one another. Figure 9 shows the heat release rate up to ignition for a SF 900 K and DF 1000 K cases. At first look, the HRR characteristics are rather similar.

Initially, LTC activates around τ_1 and it is the primary source of heat release for a certain period of time. When approaching τ_2 , high-temperature chemistry in the rich region inside the spray starts to contribute more to the heat release, HTC contribution exceeding LTC around the time of τ_2 . Hence, the figure shows that controlling the global characteristics of the ignition process is possible by changing the ambient temperature.

For SF 900 K and DF 1000 K cases, the conditional means and the standard deviations of the key species and quantities related to ignition are provided in Fig. 10. Complementing Fig. 9, heat release is noted to initiate with LTC at lean conditions, and to progress towards richer mixtures. On the contrary, HTC heat release initiates around $Z = 0.1$ and then moves towards leaner mixtures, stabilizing around stoichiometry. The peak at the Z_{st} denotes the initial high temperature ignition kernels. Composition of CH_3 and CH_4 on the other hand indicates the differences between the two cases. For SF 900 K, there is net production of CH_4 in richer conditions originating from oxidation of *n*-dodecane. In contrast, for DF 1000K, there is net consumption of ambient CH_4 originating from the rich spray regions in LTC, which then evolve to leaner conditions in the HTC regime. In general, CH_3 is a direct product of CH_4 oxidation. For the SF case, CH_3 production is initiated and maintained in rich conditions (i.e. spray region), indicating the source of CH_3 to be diesel surrogate oxidation process. For the DF case, the initiation is still at rich conditions, but it spreads to both lean and rich mixture fraction values in time. Thus, for DF, the CH_3 formation is originated both from diesel surrogate oxidation and ambient CH_4 near the spray periphery.

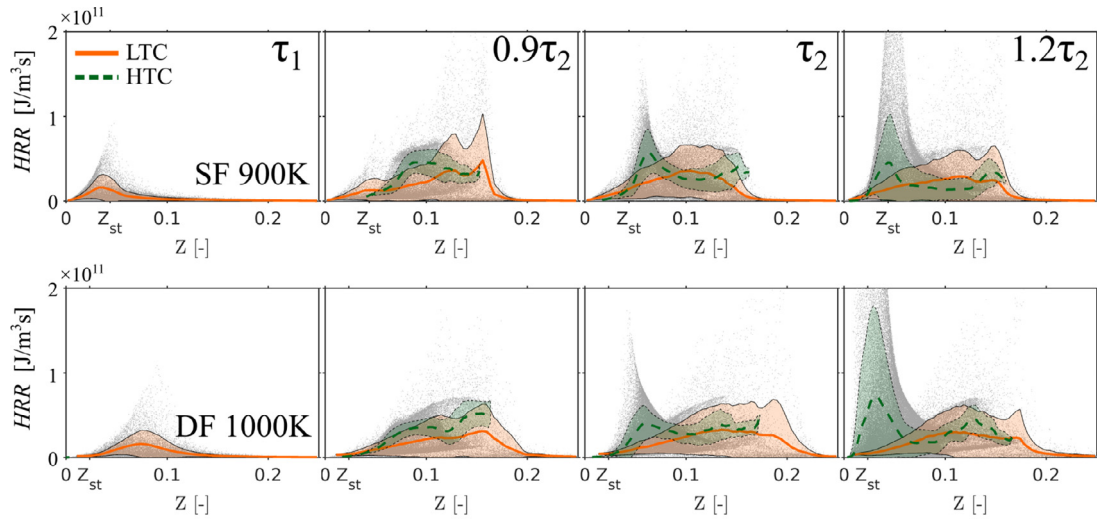
3.4. Reaction sensitivity analysis of DF mixtures

Recent studies by Kahila et al. [26] and Srna et al. [35,36] show the inhibiting influence of methane on the ignition chemistry originating from chemical kinetics. Changes in thermodynamical properties caused by methane addition in a DF mixture (e.g. specific heat) were reported to account for only ~1% of the observed IDT variations [26]. Therefore, to extend the analysis by Kahila et al. and to further explain the observed sensitivity of IDT to temperature, a brute-force sensitivity analysis was conducted.

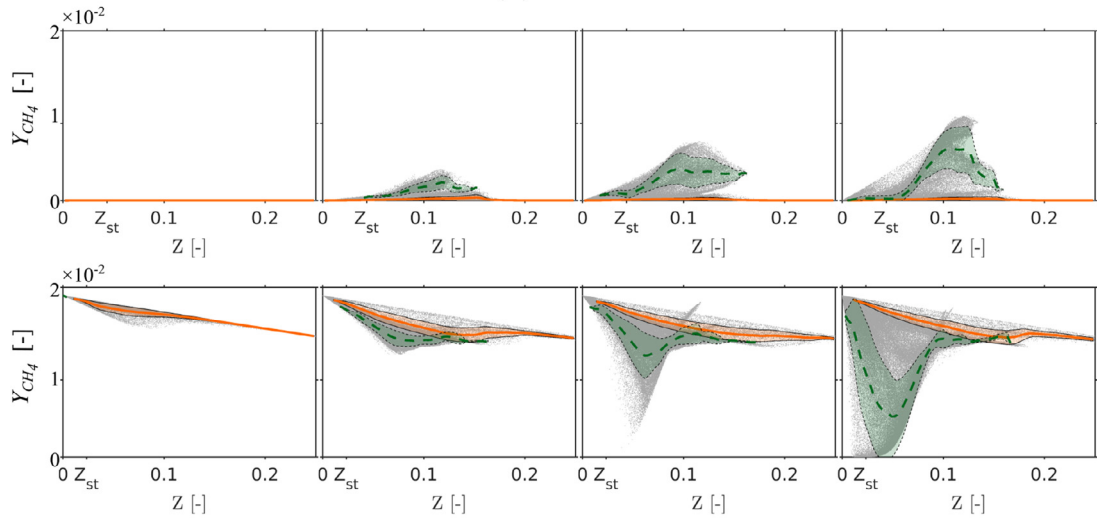
The following analysis reveals the influence of ambient temperature on the chemical pathways of *n*-dodecane/ CH_4 chemistry and particularly production/consumption rates of intermediate species such as OH, CH_3 , HO_2 and early decomposition products of *n*-dodecane such as RO_2 . In addition, the analysis suggests that inhibiting reactions related to CH_4 oxidation generally become more dominant at low temperatures, compared to reactions including long hydrocarbons originating from *n*-dodecane decomposition.

The sensitivity analysis includes OD HR computations in three different mixture compositions, corresponding to the overall equivalence ratio of $\phi = 0.5$, $\phi = 1.0$ and Z_{MR} , which are sampled from the adiabatic mixing line. The sensitivity coefficients S_i are defined as the relative change in the corresponding second-stage IDT when a specific reaction rate is multiplied by a factor of two [26,69,71]. While negative sensitivity coefficients stand for enhancing influence (i.e. decreasing IDT), the positive coefficients mean inhibiting effect (i.e. increasing IDT).

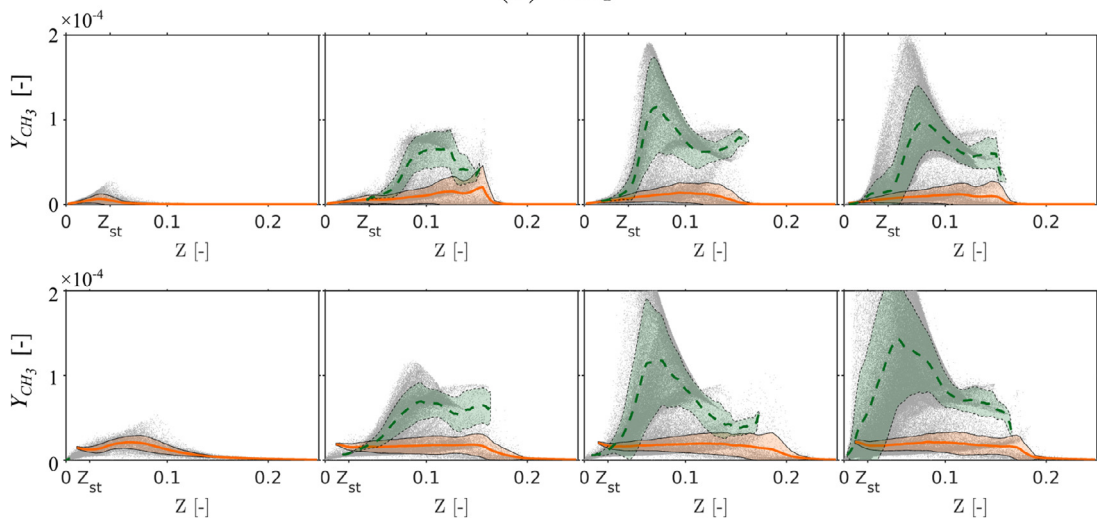
Figure 11 shows the sensitivity analysis for the DF mixtures at temperatures 1000, 900 and 850 K. Figure 11(a) and (b) follows the previously reported results [26], showing the appearance of the inhibiting reaction $\text{CH}_4 + \text{OH} \Rightarrow \text{CH}_3 + \text{H}_2\text{O}$ which produces methyl radicals and water from methane via H abstraction. Such an increased methyl radical production subsequently leads to the recombination reaction $2 \text{CH}_3(+M) \Rightarrow \text{C}_2\text{H}_6(+M)$ and to the chain terminating reaction $\text{CH}_3 + \text{HO}_2 \Rightarrow \text{CH}_4 + \text{O}_2$. Both reactions are strongly inhibiting [49,80]. In addition, the prescribed reactions consume OH and HO_2 radicals which are frequently



(a) HRR



(b) CH_4



(c) CH_3

Fig. 10. Conditional mean (solid line) and standard deviation (filled area) of (a) HRR, (b) CH_4 and (c) CH_3 with respect to Z for SF 900 K (top) and DF 1000 K (bottom). While orange color (—) denotes LTC region, HTC region is represented with green color (---). Note: only 1% of the LES data is used for background scatter by uniform sampling. (For interpretation of the references to color in this figure legend, the reader is referred to the web version of this article.)

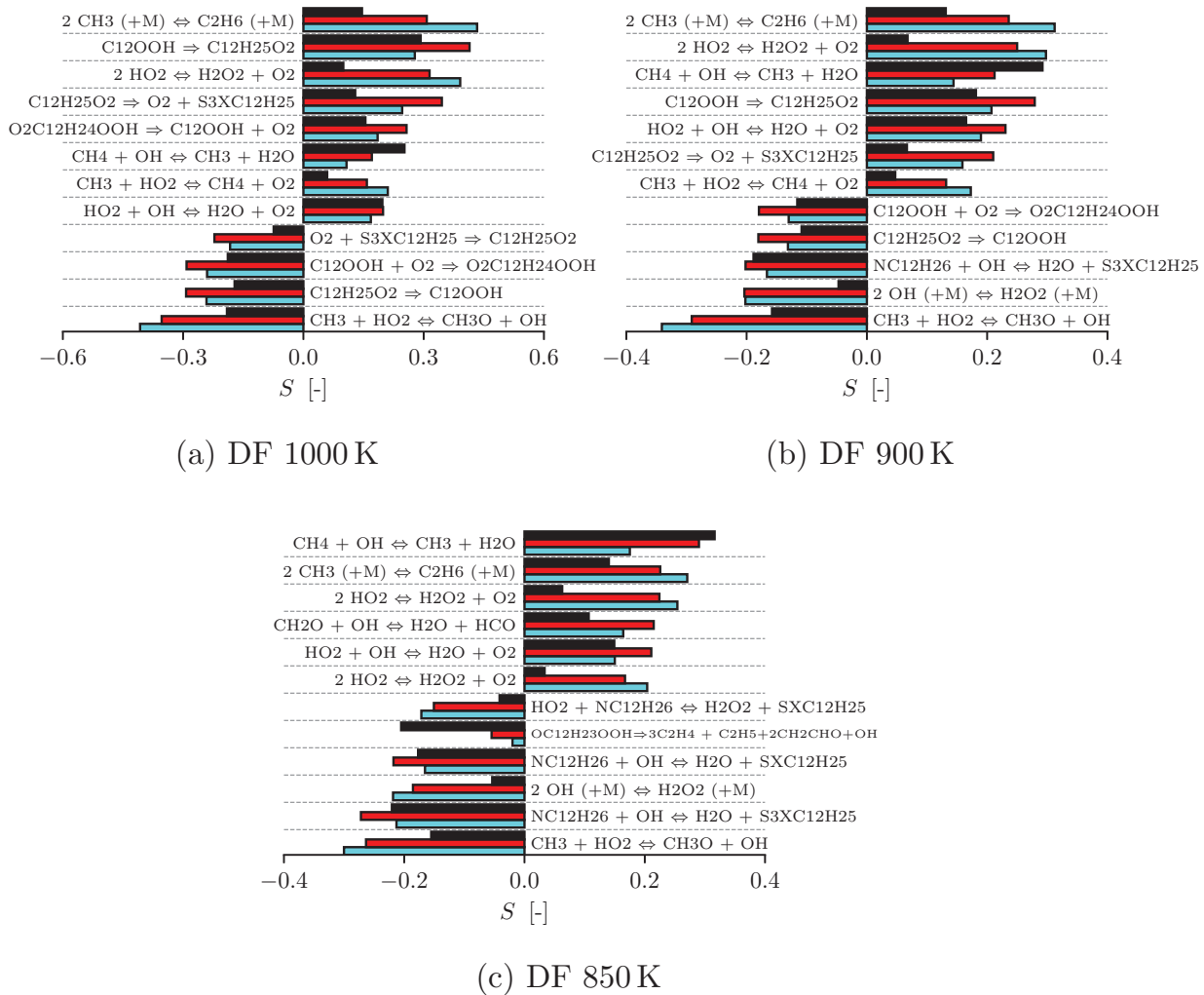


Fig. 11. Sensitivity analysis with respect to the second-stage IDT in three mixture compositions corresponding to Z_{MR} (■), Z_{st} (■) and $Z_{\phi=0.5}$ (■).

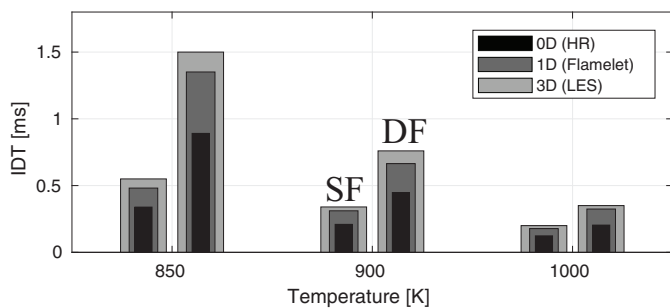


Fig. 12. A bar graph summarizing the obtained IDT results throughout the study, with the Yao mechanism. For each temperature point, left hand side bar shows SF while right hand side bar shows DF.

participating in LTC reactions as reactants (e.g. the H abstraction: $NC_{12}H_{26} + OH \Rightarrow H_2O + C_{12}H_{25}O_2$), increasing the inhibiting effect of CH_4 addition. Otherwise, the reactions shown in Fig. 11(a) and (b) are similar to the equivalent SF cases [26,71].

Comparison of the three temperatures shows that the number of reactions involving n -dodecane and its long hydrocarbon radical

products decreases as a function of mixture temperature, see Fig. 11(c). In particular, the inhibiting reactions $C_{12}OOH \Rightarrow C_{12}H_{25}O_2$ and $C_{12}H_{25}O_2 \Rightarrow O_2 + S_3XC_{12}H_{25}$ are not present for 850 K. In addition, the number of IDT promoting reactions (neg. S_i) where n -dodecane is present increases at $T = 850$ K.

Such observations on DF oxidation indicate the importance of early decomposition process of both fuels and subsequent interaction between produced intermediate species. It is worth noting that the presented analysis shows results only for the Yao mechanism. We note that, as shown by Kahila et al. [26], the influence of CH_4 on n -dodecane oxidation depends on the chosen chemical mechanism.

4. Conclusions

In this paper, we investigated the ignition characteristics of n -dodecane sprays in a lean methane–air mixture for different ambient temperature conditions using 0D, 1D and 3D simulations. The Engine Combustion Network Spray A case is employed as a single-fuel diesel ignition baseline. The case is then extended to dual-fuel configurations. Comprehensive information on ignition characteristics of dual-fuel sprays was obtained at different ambient temperatures. An overall summary of the main IDT results is presented in Fig. 12. Clearly, by accounting for mixing in higher dimensional studies, IDT is consistently prolonged. Based on the simulation

results, such a trend is noted to be the strongest at 850 K, due to the increased ratio between IDT and mixing timescales.

The main results of the paper are:

1. 0D and 1D simulations indicate that the choice of the chemical mechanism is crucial for estimating ignition characteristics, particularly at temperatures below 900 K for the present setups. In DF context, the choice of the mechanism was shown to become even more important than in SF. In particular, the effect of chemical mechanism on the IDT in 1D flamelet simulations is observed to be less than 0.05 ms for temperatures above 900 K, while this discrepancy increases up to 0.25 ms for lower temperatures (e.g. 850 K).
2. 0D, 1D and 3D simulations all support and bring further insight to the works by Srna et al. [35,36] and Kahila et al. [26,27]. The results indicate that methane prolongs both the low and high temperature ignition delay times (τ_1 and τ_2) for a range of temperatures. It is also observed that this retarding effect increases for lower temperatures. For LES simulations, the inhibiting effect of methane increases from 2 to 3.2 times for τ_1 and 1.7 to 3.1 times for τ_2 for $1000\text{ K} \geq T \geq 850\text{ K}$. In addition, within DF context, the τ_1 increases by a factor of 7.5 (0.16 to 1.21 ms), while τ_{ind} changes much less (0.20 to 0.29 ms) for $1000\text{ K} \geq T \geq 850\text{ K}$.
3. The chemical induction time τ_{ind} ($\tau_2 - \tau_1$) is shown to be less dependent on the temperature and methane addition effects compared to e.g. τ_1 . For 3D simulations, τ_{ind} changes slightly (0.02 to 0.09 ms) with ambient temperature, and increases around 0.1 to 0.15 ms in DF configurations, compared to SF.
4. The chemical sensitivity analysis indicates that reactions involving methane or methane decomposition products become more pronounced at lower temperatures, while the number of dominating reactions involving long hydrocarbons decreases. Such observation explains on its part why IDT_{DF} is strongly increasing for lower temperatures.

In practice, engine in-cylinder temperature is a function of the piston position (crank angle) and the intake air temperature. Hence, depending on the operating conditions, the ambient conditions into which the spray is injected can vary to a great extent. As seen from the sensitivity analysis, the share of inhibiting long hydrocarbon reactions decreases at lower temperatures, indicating a change in not only IDT, but also overall ignition chemistry at these conditions. Hence, in any dual-fuel application, the role of low-temperature reactions should be carefully considered when modeling ignition. This aspect may become particularly important for modern low-temperature combustion strategies (e.g. RCCI) involving early fuel injection. For such applications, the dynamic change in temperature and other thermodynamic properties during compression should be taken into account to accurately model the ignition process.

Declaration of Competing Interest

The authors declare that they have no known competing financial interests or personal relationships that could have appeared to influence the work reported in this paper.

Acknowledgments

This study has been financially supported by the [Academy of Finland](#) (Grant nos. [289592](#) and [318024](#)). The computational resources required by this study were provided by CSC – Finnish IT Center for Science. The first author has been financially supported by the Merenkulun Säätiö. The authors of this article received support from the Energy Platform at Aalto University in creating some of the featured visualizations.

Supplementary material

Supplementary material associated with this article can be found, in the online version, at doi:[10.1016/j.combustflame.2020.01.017](https://doi.org/10.1016/j.combustflame.2020.01.017).

References

- [1] R.D. Reitz, Directions in internal combustion engine research, *Combust. Flame* 160 (1) (2013) 1–8, doi:[10.1016/j.combustflame.2012.11.002](https://doi.org/10.1016/j.combustflame.2012.11.002).
- [2] R.D. Reitz, G. Duraisamy, Review of high efficiency and clean reactivity controlled compression ignition (RCCI) combustion in internal combustion engines, *Progr. Energy Combust. Sci.* 46 (2015) 12–71, doi:[10.1016/j.pecs.2014.05.003](https://doi.org/10.1016/j.pecs.2014.05.003).
- [3] S.L. Kokjohn, R.M. Hanson, D.A. Splitter, R.D. Reitz, Fuel reactivity controlled compression ignition (RCCI): a pathway to controlled high-efficiency clean combustion, *Int. J. Engine Res.* 12 (3) (2011) 209–226, doi:[10.1177/1468087411401548](https://doi.org/10.1177/1468087411401548).
- [4] D.E. Nieman, A.B. Dempsey, R.D. Reitz, Heavy-duty RCCI operation using natural gas and diesel, *SAE Int. J. Engines* 5 (2) (2012), doi:[10.4271/2012-01-0379](https://doi.org/10.4271/2012-01-0379).
- [5] B.B. Sahoo, N. Sahoo, U.K. Saha, Effect of engine parameters and type of gaseous fuel on the performance of dual-fuel gas diesel engines – a critical review, *Renew. Sustain. Energy Rev.* 13 (6–7) (2009) 1151–1184, doi:[10.1016/j.rser.2008.08.003](https://doi.org/10.1016/j.rser.2008.08.003).
- [6] J. Li, W. Yang, D. Zhou, Review on the management of RCCI engines, *Renew. Sustain. Energy Rev.* 69 (2017) 65–79, doi:[10.1016/j.rser.2016.11.159](https://doi.org/10.1016/j.rser.2016.11.159).
- [7] R.G. Papagiannakis, D.T. Hountalas, C.D. Rakopoulos, Theoretical study of the effects of pilot fuel quantity and its injection timing on the performance and emissions of a dual fuel diesel engine, *Energy Convers. Manag.* 48 (11) (2007) 2951–2961, doi:[10.1016/j.enconman.2007.07.003](https://doi.org/10.1016/j.enconman.2007.07.003).
- [8] Engine Combustion Network, Combustion Research Facility, Sandia National Laboratories, Livermore, CA.
- [9] L.M. Pickett, C.L. Genzale, G. Bruneaux, L.-M. Malbec, L. Hermant, C. Christiansen, J. Schramm, Comparison of diesel spray combustion in different high-temperature, high-pressure facilities, *SAE Int. J. Engines* 3 (2) (2010) 2010-01-2106, doi:[10.4271/2010-01-2106](https://doi.org/10.4271/2010-01-2106).
- [10] N. Maes, M. Meijer, N. Dam, B. Somers, H. Baya Toda, G. Bruneaux, S.A. Skeen, L.M. Pickett, J. Manin, Characterization of Spray A flame structure for parametric variations in ECN constant-volume vessels using chemiluminescence and laser-induced fluorescence, *Combust. Flame* 174 (2016) 138–151, doi:[10.1016/j.combustflame.2016.09.005](https://doi.org/10.1016/j.combustflame.2016.09.005).
- [11] S. Skeen, J. Manin, L.M. Pickett, Visualization of ignition processes in high-pressure sprays with multiple injections of n-dodecane, *SAE Int. J. Engines* 8 (2) (2015) 2015-01-0799, doi:[10.4271/2015-01-0799](https://doi.org/10.4271/2015-01-0799).
- [12] S.A. Skeen, J. Manin, L.M. Pickett, Simultaneous formaldehyde PLIF and high-speed schlieren imaging for ignition visualization in high-pressure spray flames, *Proc. Combust. Inst.* 35 (3) (2015) 3167–3174, doi:[10.1016/j.proci.2014.06.040](https://doi.org/10.1016/j.proci.2014.06.040).
- [13] J. Benajes, R. Payri, M. Bardi, P. Martí-Aldaraví, Experimental characterization of diesel ignition and lift-off length using a single-hole ECN injector, *Appl. Therm. Eng.* 58 (1–2) (2013) 554–563, doi:[10.1016/j.applthermaleng.2013.04.044](https://doi.org/10.1016/j.applthermaleng.2013.04.044).
- [14] Y. Pei, S. Som, P. Kundu, G.M. Goldin, Large Eddy Simulation of a Reacting Spray Flame under Diesel Engine Conditions, *SAE Technical Paper*(2015-01-1844) (2015), doi:[10.4271/2015-01-1844](https://doi.org/10.4271/2015-01-1844).
- [15] Y. Pei, M.J. Davis, L.M. Pickett, S. Som, Engine combustion network (ECN): global sensitivity analysis of Spray A for different combustion vessels, *Combust. Flame* 162 (6) (2015) 2337–2347, doi:[10.1016/j.combustflame.2015.01.024](https://doi.org/10.1016/j.combustflame.2015.01.024).
- [16] A. Wehrfritz, V. Vuorinen, O. Kaario, M. Larmi, Large eddy simulation of high-velocity fuel sprays: studying mesh resolution and breakup model effects for Spray A, *Atom. Sprays* 23 (5) (2013) 419–442, doi:[10.1615/AtomizSpr.2013007342](https://doi.org/10.1615/AtomizSpr.2013007342).
- [17] M. Bolla, M.A. Chishty, E.R. Hawkes, S. Kook, Modeling combustion under engine combustion network Spray A conditions with multiple injections using the transported probability density function method, *Int. J. Engine Res.* 18 (1–2) (2017) 6–14, doi:[10.1177/1468087416689174](https://doi.org/10.1177/1468087416689174).
- [18] Y. Pei, B. Hu, S. Som, Large-eddy simulation of an n-dodecane spray flame under different ambient oxygen conditions, *J. Energy Resour. Technol.* 138 (3) (2016) 032205, doi:[10.1115/1.4032771](https://doi.org/10.1115/1.4032771).
- [19] H. Kahila, A. Wehrfritz, O. Kaario, M. Ghaderi Masouleh, N. Maes, B. Somers, V. Vuorinen, Large-eddy simulation on the influence of injection pressure in reacting Spray A, *Combust. Flame* 191 (2018) 142–159, doi:[10.1016/j.combustflame.2018.01.004](https://doi.org/10.1016/j.combustflame.2018.01.004).
- [20] C. Xu, M.M. Ameen, S. Som, J.H. Chen, Z. Ren, T. Lu, Dynamic adaptive combustion modeling of spray flames based on chemical explosive mode analysis, *Combust. Flame* 195 (2018) 30–39, doi:[10.1016/j.combustflame.2018.05.019](https://doi.org/10.1016/j.combustflame.2018.05.019).
- [21] Y. Pei, S. Som, E. Pomraning, P.K. Senecal, S.A. Skeen, J. Manin, L.M. Pickett, Large eddy simulation of a reacting spray flame with multiple realizations under compression ignition engine conditions, *Combust. Flame* 162 (12) (2015) 4442–4455, doi:[10.1016/j.combustflame.2015.08.010](https://doi.org/10.1016/j.combustflame.2015.08.010).
- [22] Y. Pei, E.R. Hawkes, S. Kook, G.M. Goldin, T. Lu, Modelling n-dodecane spray and combustion with the transported probability density function method,

- Combust. Flame 162 (5) (2015) 2006–2019, doi:[10.1016/j.combustflame.2014.12.019](https://doi.org/10.1016/j.combustflame.2014.12.019).
- [23] Y. Pei, E.R. Hawkes, M. Bolla, S. Kook, G.M. Goldin, Y. Yang, S.B. Pope, S. Som, An analysis of the structure of an n-dodecane spray flame using TPDF modelling, *Combust. Flame* 168 (2016) 420–435, doi:[10.1016/j.combustflame.2015.11.034](https://doi.org/10.1016/j.combustflame.2015.11.034).
- [24] M.M. Ameen, P. Kundu, S. Som, Novel tabulated combustion model approach for lifted spray flames with large eddy simulations, *SAE Int. J. Engines* 9 (4) (2016) 2016–01–2194, doi:[10.4271/2016-01-2194](https://doi.org/10.4271/2016-01-2194).
- [25] P. Kundu, M.M. Ameen, S. Som, Importance of turbulence-chemistry interactions at low temperature engine conditions, *Combust. Flame* 183 (2017) 283–298, doi:[10.1016/j.combustflame.2017.05.025](https://doi.org/10.1016/j.combustflame.2017.05.025).
- [26] H. Kahila, A. Wehrfritz, O. Kaario, V. Vuorinen, Large-eddy simulation of dual-fuel ignition: diesel spray injection into a lean methane-air mixture, *Combust. Flame* 199 (2019) 131–151, doi:[10.1016/j.combustflame.2018.10.014](https://doi.org/10.1016/j.combustflame.2018.10.014).
- [27] H. Kahila, O. Kaario, Z. Ahmad, M. Ghaderi Masouleh, B. Tekgül, M. Larmi, V. Vuorinen, A large-eddy simulation study on the influence of diesel pilot spray quantity on methane-air flame initiation, *Combust. Flame* 206 (2019) 506–521, doi:[10.1016/j.combustflame.2019.05.025](https://doi.org/10.1016/j.combustflame.2019.05.025).
- [28] G.H. Abd Alla, H.A. Soliman, O.A. Badr, M.F. Abd Rabbo, Effect of injection timing on the performance of a dual fuel engine, *Energy Convers. Manag.* 43 (2) (2002) 269–277, doi:[10.1016/S0196-8904\(00\)00168-0](https://doi.org/10.1016/S0196-8904(00)00168-0).
- [29] G.A. Karim, Combustion in gas fueled compression: ignition engines of the dual fuel type, *J. Eng. Gas Turb. Power* 125 (3) (2003) 827, doi:[10.1115/1.1581894](https://doi.org/10.1115/1.1581894).
- [30] Z. Ahmad, J. Aryal, O. Ranta, O. Kaario, V. Vuorinen, M. Larmi, An Optical Characterization of Dual-Fuel Combustion in a Heavy-Duty Diesel Engine, 2018, doi:[10.4271/2018-01-0252](https://doi.org/10.4271/2018-01-0252). Abstract. SAE Technical Paper
- [31] J. Liu, F. Yang, H. Wang, M. Ouyang, S. Hao, Effects of pilot fuel quantity on the emissions characteristics of a CNG/diesel dual fuel engine with optimized pilot injection timing, *Appl. Energy* 110 (2013) 201–206, doi:[10.1016/j.apenergy.2013.03.024](https://doi.org/10.1016/j.apenergy.2013.03.024).
- [32] G.A. Karim, A review of combustion processes in the dual fuel engine – the gas diesel engine, *Progr. Energy Combust. Sci.* 6 (3) (1980) 277–285, doi:[10.1016/0360-1285\(80\)90019-2](https://doi.org/10.1016/0360-1285(80)90019-2).
- [33] L. Wei, P. Geng, A review on natural gas/diesel dual fuel combustion, emissions and performance, *Fuel Process. Technol.* 142 (2016) 264–278, doi:[10.1016/j.fuproc.2015.09.018](https://doi.org/10.1016/j.fuproc.2015.09.018).
- [34] S. Schlatter, B. Schneider, Y.M. Wright, K. Boulouchos, N-heptane micro pilot assisted methane combustion in a rapid compression expansion machine, *Fuel* 179 (2016) 339–352, doi:[10.1016/j.fuel.2016.03.006](https://doi.org/10.1016/j.fuel.2016.03.006).
- [35] A. Srna, B. von Rotz, K. Herrmann, K. Boulouchos, G. Bruneaux, Experimental investigation of pilot-fuel combustion in dual-fuel engines, Part 1: thermodynamic analysis of combustion phenomena, *Fuel* (2019) 115642, doi:[10.1016/j.fuel.2019.115642](https://doi.org/10.1016/j.fuel.2019.115642).
- [36] A. Srna, B. von Rotz, M. Bolla, Y.M. Wright, K. Herrmann, K. Boulouchos, G. Bruneaux, Experimental investigation of pilot-fuel combustion in dual-fuel engines, Part 2: understanding the underlying mechanisms by means of optical diagnostics, *Fuel* (2019) 115766, doi:[10.1016/j.fuel.2019.115766](https://doi.org/10.1016/j.fuel.2019.115766).
- [37] J.J. López, R. Novella, A. García, J.F. Winklinger, Investigation of the ignition and combustion processes of a dual-fuel spray under diesel-like conditions using computational fluid dynamics (CFD) modeling, *Math. Comput. Model.* 57 (7–8) (2013) 1897–1906, doi:[10.1016/j.mcm.2011.12.030](https://doi.org/10.1016/j.mcm.2011.12.030).
- [38] S. Hu, C. Gong, X.S. Bai, Dual fuel combustion of n-heptane/methanol-air-EGR mixtures, *Energy Procedia*, 105, Elsevier (2017), pp. 4943–4948, doi:[10.1016/j.egypro.2017.03.986](https://doi.org/10.1016/j.egypro.2017.03.986).
- [39] A. Maghbouli, R.K. Saray, S. Shafee, J. Ghafouri, Numerical study of combustion and emission characteristics of dual-fuel engines using 3D-CFD models coupled with chemical kinetics, *Fuel* 106 (2013) 98–105, doi:[10.1016/j.fuel.2012.10.055](https://doi.org/10.1016/j.fuel.2012.10.055).
- [40] Y. Li, M. Jia, Y. Chang, Y. Liu, M. Xie, T. Wang, L. Zhou, Parametric study and optimization of a RCCI (reactivity controlled compression ignition) engine fueled with methanol and diesel, *Energy* 65 (2014) 319–332, doi:[10.1016/j.energy.2013.11.059](https://doi.org/10.1016/j.energy.2013.11.059).
- [41] A. Bhagatwala, R. Sankaran, S. Kokjohn, J.H. Chen, Numerical investigation of spontaneous flame propagation under RCCI conditions, *Combust. Flame* 162 (9) (2015) 3412–3426, doi:[10.1016/j.combustflame.2015.06.005](https://doi.org/10.1016/j.combustflame.2015.06.005).
- [42] E. Demosthenous, G. Borghesi, E. Mastorakos, R.S. Cant, Direct numerical simulations of premixed methane flame initiation by pilot n-heptane spray auto-ignition, *Combust. Flame* 163 (2016) 122–137, doi:[10.1016/j.combustflame.2015.09.013](https://doi.org/10.1016/j.combustflame.2015.09.013).
- [43] A. Talekar, M. Lai, E. Tomita, N. Kawahara, et al., Numerical Investigation of Natural Gas-Diesel Dual Fuel Engine With End Gas Ignition, 2018, doi:[10.4271/2018-01-0199](https://doi.org/10.4271/2018-01-0199). SAE Technical Papers
- [44] A. Jamali, M.R. Nalim, Numerical simulation of dual-fuel compression-ignition engine in part-load operating condition with double injection, *Proceedings of the ASME 2016 Internal Combustion Engine Fall Technical Conference, ICEF2016* (2016), pp. 1–8. October 9–12, 2016. doi:[10.1115/ICEF2016-9374](https://doi.org/10.1115/ICEF2016-9374).
- [45] G.H. Abd Alla, H.A. Soliman, O.A. Badr, M.F. Abd Rabbo, Combustion quasi-two zone predictive model for dual fuel engines, *Energy Convers. Manag.* 42 (12) (2001) 1477–1498, doi:[10.1016/S0196-8904\(00\)00143-6](https://doi.org/10.1016/S0196-8904(00)00143-6).
- [46] Z. Ahmad, O. Kaario, C. Qiang, V. Vuorinen, M. Larmi, A parametric investigation of diesel/methane dual-fuel combustion progression/stages in a heavy-duty optical engine, *Appl. Energy* 251 (2019) 113191, doi:[10.1016/j.apenergy.2019.04.187](https://doi.org/10.1016/j.apenergy.2019.04.187).
- [47] M. Grochowina, M. Schiffrer, S. Tartsch, T. Sattelmayer, Influence of injection parameters and operating conditions on ignition and combustion in dual-fuel engines, *J. Eng. Gas Turb. Power* 140 (10) (2018) 102809, doi:[10.1115/1.4040089](https://doi.org/10.1115/1.4040089).
- [48] M. Ghaderi Masouleh, A. Wehrfritz, O. Kaario, H. Kahila, V. Vuorinen, Comparative study on chemical kinetic schemes for dual-fuel combustion of n-dodecane/methane blends, *Fuel* 191 (2017) 62–76, doi:[10.1016/j.fuel.2016.10.114](https://doi.org/10.1016/j.fuel.2016.10.114).
- [49] D.M. Manias, E.A. Tingas, C.E. Frouzakis, K. Boulouchos, D.A. Goussis, The mechanism by which CH₂O and H₂O₂ additives affect the autoignition of CH₄/air mixtures, *Combust. Flame* 164 (2016) 111–125, doi:[10.1016/j.combustflame.2015.11.008](https://doi.org/10.1016/j.combustflame.2015.11.008).
- [50] A. Srna, M. Bolla, Y.M. Wright, K. Herrmann, R. Bombach, S.S. Pandurangi, K. Boulouchos, G. Bruneaux, Effect of methane on pilot-fuel auto-ignition in dual-fuel engines, *Proc. Combust. Inst.* (2018), doi:[10.1016/j.proci.2018.06.177](https://doi.org/10.1016/j.proci.2018.06.177).
- [51] H.G. Weller, G. Tabor, H. Jasak, C. Fureby, A tensorial approach to computational continuum mechanics using object-oriented techniques, *Comput. Phys.* 12 (6) (1998) 620, doi:[10.1063/1.168744](https://doi.org/10.1063/1.168744).
- [52] H. Jasak, H.G. Weller, A.D. Gosman, High resolution NVD differencing scheme for arbitrarily unstructured meshes, *Int. J. Numer. Methods Fluids* 31 (2) (1999) 431–449, doi:[10.1002/\(SICI\)1097-0363\(19990930\)31:2<431::AID-FLD884>3.0.CO;2-T](https://doi.org/10.1002/(SICI)1097-0363(19990930)31:2<431::AID-FLD884>3.0.CO;2-T).
- [53] A. Wehrfritz, O. Kaario, V. Vuorinen, B. Somers, Large eddy simulation of n-dodecane spray flames using flamelet generated manifolds, *Combust. Flame* 167 (2016) 113–131, doi:[10.1016/j.combustflame.2016.02.019](https://doi.org/10.1016/j.combustflame.2016.02.019).
- [54] R.D. Reitz, Modeling atomization processes in high-pressure vaporizing sprays, *Atom. Sprays* 3 (1987) 309–337.
- [55] R.D. Reitz, J.C. Beale, Modeling spray atomization with the Kelvin-Helmholtz/Rayleigh-Taylor hybrid model, *Atom. Sprays* 9 (6) (1999) 623–650, doi:[10.1615/AtomizSpr.v9.i6.40](https://doi.org/10.1615/AtomizSpr.v9.i6.40).
- [56] N. Frössling, Evaporation, heat transfer and velocity distribution in two-dimensional and Rotationally Symmetrical Laminar Boundary-Layer Flow. N.A.C.A. ADB1891., 1956 Technical Report.
- [57] W.E. Ranz, W.R. Marshall, Evaporation from drops – Part 1, *Chem. Eng. Progr.* 48 (1952) 141–148, doi:[10.1016/S0924-7963\(01\)00032-X](https://doi.org/10.1016/S0924-7963(01)00032-X).
- [58] W.E. Ranz, W.R. Marshall, Evaporation from drops – Part 2, *Chem. Eng. Progr.* 48 (1952) 173–180.
- [59] K.E. Niemeyer, N.J. Curtis, C.J. Sung, pyjac: analytical Jacobian generator for chemical kinetics, *Comput. Phys. Commun.* 215 (2017) 188–203, doi:[10.1016/j.cpc.2017.02.004](https://doi.org/10.1016/j.cpc.2017.02.004).
- [60] E. Hairer, G. Wanner, *Solving Ordinary Differential Equations II*, 14, Springer-Verlag, 1996, doi:[10.1007/978-3-662-09947-6](https://doi.org/10.1007/978-3-662-09947-6).
- [61] C. Duwig, K.J. Nogenmyr, C.K. Chan, M.J. Dunn, Large eddy simulations of a piloted lean premix jet flame using finite-rate chemistry, *Combust. Theory Model.* 15 (4) (2011) 537–568, doi:[10.1080/13647830.2010.548531](https://doi.org/10.1080/13647830.2010.548531).
- [62] C. Eberle, P. Gerlinger, K.P. Geigle, M. Aigner, Toward finite-rate chemistry large-eddy simulations of sooting swirl flames, 2018, doi:[10.1080/00102202.2018.1443444](https://doi.org/10.1080/00102202.2018.1443444).
- [63] J.A. Fulton, J.R. Edwards, A. Cutler, J. McDaniel, C. Goyne, Turbulence/chemistry interactions in a ramp-stabilized supersonic hydrogen air diffusion flame, *Combust. Flame* 174 (2016) 152–165, doi:[10.1016/j.combustflame.2016.09.017](https://doi.org/10.1016/j.combustflame.2016.09.017).
- [64] E.R. Hawkes, B. Somers, *Ignition and flame structure – model results & analysis (in Spray A)*, 5th Engine Combustion Network Workshop (2017). Detroit, MI, USA
- [65] A. Wehrfritz, B. Savard, E. Hawkes, Comparison of chemical mechanisms for n-dodecane at engine conditions using an unsteady flamelet model, 11th Asia-Pacific Conference on Combustion (2017), pp. 10–13, doi:[10.1111/j.1468-0408.1992.tb00434.x](https://doi.org/10.1111/j.1468-0408.1992.tb00434.x). 2017-Decem
- [66] S.M. Sarathy, C.K. Westbrook, M. Mehl, W.J. Pitz, C. Togbe, P. Dagaut, H. Wang, M.A. Oehlschlaeger, U. Niemann, K. Seshadri, P.S. Veloo, C. Ji, F.N. Egolfopoulos, T. Lu, Comprehensive chemical kinetic modeling of the oxidation of 2-methylalkanes from C7 to C20, *Combust. Flame* 158 (12) (2011) 2338–2357, doi:[10.1016/j.combustflame.2011.05.007](https://doi.org/10.1016/j.combustflame.2011.05.007).
- [67] E. Ranzi, A. Frassoldati, R. Grana, A. Cuoci, T. Faravelli, A.P. Kelley, C.K. Law, Hierarchical and comparative kinetic modeling of laminar flame speeds of hydrocarbon and oxygenated fuels, *Progr. Energy Combust. Sci.* 38 (4) (2012) 468–501, doi:[10.1016/j.pecs.2012.03.004](https://doi.org/10.1016/j.pecs.2012.03.004).
- [68] E. Ranzi, A. Frassoldati, A. Stagni, M. Pelucchi, A. Cuoci, T. Faravelli, Reduced kinetic schemes of complex reaction systems: fossil and biomass-derived transportation fuels, *Int. J. Chem. Kinet.* 46 (9) (2014) 512–542, doi:[10.1002/kin.20867](https://doi.org/10.1002/kin.20867).
- [69] K. Narayanaswamy, P. Pepiot, H. Pitsch, A chemical mechanism for low to high temperature oxidation of n-dodecane as a component of transportation fuel surrogates, *Combust. Flame* 161 (4) (2014) 866–884, doi:[10.1016/j.combustflame.2013.10.012](https://doi.org/10.1016/j.combustflame.2013.10.012).
- [70] Z. Luo, S. Som, S.M. Sarathy, M. Plomer, W.J. Pitz, D.E. Longman, T. Lu, Development and validation of an n-dodecane skeletal mechanism for spray combustion applications, *Combust. Theory Model.* 18 (2) (2014) 187–203, doi:[10.1080/13647830.2013.872807](https://doi.org/10.1080/13647830.2013.872807).
- [71] T. Yao, Y. Pei, B.J. Zhong, S. Som, T. Lu, K.H. Luo, A compact skeletal mechanism for n-dodecane with optimized semi-global low-temperature chemistry for diesel engine simulations, *Fuel* 191 (2017) 339–349, doi:[10.1016/j.fuel.2016.11.083](https://doi.org/10.1016/j.fuel.2016.11.083).
- [72] A. Frassoldati, G. D'Errico, T. Lucchini, A. Stagni, A. Cuoci, T. Faravelli, A. Onorati, E. Ranzi, Reduced kinetic mechanisms of diesel fuel surrogate for engine

- CFD simulations, *Combust. Flame* 162 (10) (2015) 3991–4007, doi:[10.1016/j.combustflame.2015.07.039](https://doi.org/10.1016/j.combustflame.2015.07.039).
- [73] T. Lu, M. Plomer, Z. Luo, S. Sarathy, W. Pitz, S. Som, D. Longman, Directed relation graph with expert knowledge for skeletal mechanism reduction, 7th U.S. National Combustion Meeting (2011), pp. 1–10.
- [74] J.M. Desantes, J.J. López, J.M. García-Oliver, D. López-Pintor, Experimental validation and analysis of seven different chemical kinetic mechanisms for n-dodecane using a rapid compression-expansion machine, *Combust. Flame* 182 (2017) 76–89, doi:[10.1016/j.combustflame.2017.04.004](https://doi.org/10.1016/j.combustflame.2017.04.004).
- [75] D. Goodwin, Cantera. An Object-Oriented Software Toolkit for Chemical Kinetics, Thermodynamics, and Transport Processes. Version 2.3.
- [76] H.J. Curran, Developing detailed chemical kinetic mechanisms for fuel combustion, *Proc. Combust. Inst.* (2018), doi:[10.1016/j.proci.2018.06.054](https://doi.org/10.1016/j.proci.2018.06.054).
- [77] G. Dixon-Lewis, T. David, P.H. Gaskell, S. Fukutani, H. Jinno, J.A. Miller, R.J. Kee, M.D. Smooke, N. Peters, E. Effelsberg, J. Warnatz, F. Behrendt, Calculation of the structure and extinction limit of a methane-air counterflow diffusion flame in the forward stagnation region of a porous cylinder, *Symp.(Int.) Combust.* 20 (1) (1985) 1893–1904, doi:[10.1016/S0082-0784\(85\)80688-3](https://doi.org/10.1016/S0082-0784(85)80688-3).
- [78] B. Somers, The simulation of flat flames with detailed and reduced chemical models, 1994 Ph.D. thesis.
- [79] Chem1D, A One-Dimensional Laminar Flame Code, Eindhoven University of Technology.
- [80] C.K. Westbrook, Chemical kinetics of hydrocarbon ignition in practical combustion systems, *Proc. Combust. Inst.* 28 (2) (2000) 1563–1577, doi:[10.1016/S0082-0784\(00\)80554-8](https://doi.org/10.1016/S0082-0784(00)80554-8).
- [81] K.D. Dahm, P.S. Virk, R. Bounaceur, F. Battin-Leclerc, P.M. Marquaire, R. Fournet, E. Daniau, M. Bouchez, Experimental and modelling investigation of the thermal decomposition of n-dodecane, *J. Anal. Appl. Pyrolysis* 71 (2) (2004) 865–881, doi:[10.1016/j.jaap.2003.11.005](https://doi.org/10.1016/j.jaap.2003.11.005).